Preprint typeset in JHEP style - PAPER VERSION

arXiv:0808.2462
MPP-2008-107

Thermal relic abundances of long-lived staus

Josef Pradler

Max-Planck-Institut für Physik, Föhringer Ring 6, D–80805 Munich, Germany
E-mail: jpradler@mppmu.mpg.de

Frank Daniel Steffen

Max-Planck-Institut für Physik, Föhringer Ring 6, D–80805 Munich, Germany
E-mail: steffen@mppmu.mpg.de

Abstract: In supersymmetric models with a long-lived stau being the lightest Standard Model superpartner, the stau abundance during primordial nucleosynthesis is tightly constrained. Considering the complete set of stau annihilation channels in the minimal supersymmetric Standard Model (MSSM) with real parameters for scenarios in which sparticle coannihilations are negligible, we calculate the decoupling of the lighter stau from the primordial plasma and identify processes which are capable to deplete the resulting stau abundance significantly. We find particularly efficient stau annihilation at the resonance of the heavy CP-even Higgs boson and for a lighter stau with a sizeable left–right mixing due to enhanced stau-Higgs couplings. Even within the constrained MSSM, we encounter both effects leading to exceptionally small values of the resulting stau abundance. Prospects for collider phenomenology are discussed and possible implications of our findings are addressed with emphasis on gravitino dark matter scenarios.

Contents

1. Introduction

The appearance of the lighter stau $\widetilde{\tau}_1$ as the lightest Standard Model superpartner—or lightest ordinary superpartner (LOSP)—is a commonplace occurrence even in supersymmetric (SUSY) models with restrictive assumptions on the SUSY breaking sector such as the constrained minimal supersymmetric Standard Model (CMSSM). If the lightest supersymmetric particle (LSP) is assumed to be the LOSP, this parameter region is not considered because of severe upper limits on the abundance of massive stable charged particles [1]. However, for example, in axino/gravitino LSP scenarios [2, 3, 4, 5, 6] and in scenarios with broken R parity [7, 8, 9, 10, 11],[1] the $\widetilde{\tau}$ LOSP becomes unstable and thereby a viable option. Indeed, supersymmetric models with a long-lived $\widetilde{\tau}_1$ LOSP are particularly promising for collider phenomenology [12, 13, 14, 15, 16, 17, 18, 19, 20, 21, 22, 23, 24]: Since the $\widetilde{\tau}_1$ LOSP could escape the collider detector as a quasi-stable muon-like particle, it can be associated with signatures that are very different from the excess in missing energy expected in neutralino LSP scenarios.

[1] In this work we assume that R-parity is conserved.

In the early Universe the negatively charged LOSP $\widetilde{\tau}_1$'s and the associated positively charged anti-staus $\widetilde{\tau}_1^*$'s were in thermal equilibrium for temperatures of $T > m_{\widetilde{\tau}_1}/20 \gtrsim T_{\rm f}$. At $T_{\rm f}$, the annihilation rate of the (by then) non-relativistic $\widetilde{\tau}_1$'s becomes smaller than the Hubble rate so that they decouple from the thermal plasma. Thus, for $T \lesssim T_{\rm f}$, their yield $Y_{\widetilde{\tau}} \equiv (n_{\widetilde{\tau}_1} + n_{\widetilde{\tau}_1^*})/s$ is given approximately by $Y_{\widetilde{\tau}} \approx Y_{\widetilde{\tau}}^{\rm eq}(T_{\rm f})$, where $n_{\widetilde{\tau}}^{\rm (eq)} \equiv n_{\widetilde{\tau}_1}^{\rm (eq)} + n_{\widetilde{\tau}_1^*}^{\rm (eq)}$ is the (equilibrium) number density of both $\widetilde{\tau}_1$ and $\widetilde{\tau}_1^*$ and $s = 2\pi^2\, g_{*S}\, T^3/45$ the entropy density with g_{*S} effective degrees of freedom. This thermal relic abundance $Y_{\widetilde{\tau}}$ is subject to cosmological constraints in SUSY scenarios with a long-lived $\widetilde{\tau}_1$ LOSP:

- In axino/gravitino LSP scenarios, $Y_{\widetilde{\tau}}$ governs the non-thermally produced (NTP) relic density of axino/gravitino dark matter that originates from $\widetilde{\tau}_1$ decays [3, 5] $\Omega_{\widetilde{\rm a}/\widetilde{G}}^{\rm NTP} h^2 = m_{\widetilde{\rm a}/\widetilde{G}}\, Y_{\widetilde{\tau}}\, s(T_0) h^2/\rho_{\rm c}$ where $m_{\widetilde{\rm a}/\widetilde{G}}$ denotes the axino/gravitino LSP mass and $\rho_c/[s(T_0)h^2] = 3.6 \times 10^{-9}\,{\rm GeV}$ [1]. Thus, the dark matter density $\Omega_{\rm dm}$ which limits $\Omega_{\widetilde{\rm a}/\widetilde{G}}^{\rm NTP}$ from above implies an upper limit on $Y_{\widetilde{\tau}}$ for a given $m_{\widetilde{\rm a}/\widetilde{G}}$. This limit can become particularly restrictive in the case of additional sizeable contributions to $\Omega_{\rm dm}$ such as the ones from thermal axino/gravitino production $\Omega_{\widetilde{\rm a}/\widetilde{G}}^{\rm TP}$ [25, 26, 27, 28]. For example, for $m_{\widetilde{\rm a}/\widetilde{G}} = 50$ GeV and $\Omega_{\widetilde{\rm a}/\widetilde{G}}^{\rm TP} = 0.99\,\Omega_{\rm dm}$ $(0.9\,\Omega_{\rm dm})$, one finds $Y_{\widetilde{\tau}} < 10^{-13}$ (10^{-12}); cf. Fig. 13 of Ref. [22].

- For $\widetilde{\tau}_1$ decays during/after big bang nucleosynthesis (BBN), the Standard Model particles emitted in addition to the axino/gravitino LSP can affect the abundances of the primordial light elements. This leads to upper limits on $\xi_{\rm em/had} \equiv \epsilon_{\rm em/had}\, Y_{\widetilde{\tau}}$ that depend on the stau lifetime $\tau_{\widetilde{\tau}_1}$ [29, 30, 31]. Here $\epsilon_{\rm em/had}$ denotes the (average) electromagnetic/hadronic energy emitted in a single $\widetilde{\tau}_1$ decay, which can be calculated with particle physics methods for a given model. Accordingly, the BBN constraints on $\xi_{\rm em/had}$ can be translated into upper limits on $Y_{\widetilde{\tau}}$; cf. Fig. 12 of Ref. [22] (and Figs. 14 and 15 of Ref. [32]) for associated $Y_{\widetilde{\tau}}$ limits in gravitino LSP scenarios, which can be as restrictive as $Y_{\widetilde{\tau}} < 10^{-14}$ (10^{-15}).

- The mere presence of the negatively charged $\widetilde{\tau}_1$'s at cosmic times of $t \gtrsim 5 \times 10^3\,{\rm s}$ can lead to $(^4{\rm He}\,\widetilde{\tau}_1)$ and $(^8{\rm Be}\,\widetilde{\tau}_1)$ bound states and can thereby allow for catalyzed BBN (CBBN) of ^{6}Li and ^{9}Be to abundances far above the ones obtained in standard BBN (SBBN) [33, 34, 35, 36]. Indeed, confronting the abundances obtained in CBBN with observationally inferred bounds on the primordial abundances of ^{9}Be (and ^{6}Li) imposes restrictive upper limits of $Y_{\widetilde{\tau}} \lesssim 2\times10^{-15}$ $(2\times10^{-15} - 2\times10^{-16})$ for $\tau_{\widetilde{\tau}_1} \gtrsim 10^5\,{\rm s}$; cf. Fig. 5 in Ref. [36] for $n_{\widetilde{\tau}_1} = n_{\widetilde{\tau}_1^*}$.

For example, in gravitino LSP scenarios with the $\widetilde{\tau}_1$ LOSP being the next-to-lightest supersymmetric particle (NLSP) and conserved R-parity, the listed cosmological constraints have been confronted with representative values [37, 38]

$$Y_{\widetilde{\tau}} \simeq (0.4 - 1.5) \times 10^{-13} \left(\frac{m_{\widetilde{\tau}_1}}{100\ {\rm GeV}}\right)\ , \tag{1.1}$$

which are in good agreement with the curves in Fig. 1 of Ref. [37] that have been obtained for the case of a purely 'right-handed' $\widetilde{\tau}_1 \simeq \widetilde{\tau}_{\rm R}$ NLSP and a bino-like lightest neutralino,

$\widetilde{\chi}_1^0 \simeq \widetilde{B}$, with a mass of $m_{\widetilde{B}} = 1.1\, m_{\widetilde{\tau}_1}$. Thereby, it has been found that the (C)BBN constraints impose the limit $\tau_{\widetilde{\tau}_1} \lesssim 5 \times 10^3$ s [33, 36] with severe implications in the collider-friendly region of $m_{\widetilde{\tau}_1} < 1$ TeV: (i) The $\tau_{\widetilde{\tau}_1}$ limit disfavors the kinematical determination of $m_{\widetilde{G}}$ [39] and thereby both the determination of the Planck scale at colliders [16] and the method proposed to probe the maximum reheating temperature $T_{\rm R}$ at colliders [27]. (ii) Within the CMSSM, the $\tau_{\widetilde{\tau}_1}$ limit implies an upper limit on the reheating temperature of $T_{\rm R} \lesssim 10^7$ GeV [40, 41, 42] that disfavors the viability of thermal leptogenesis with hierarchical heavy Majorana neutrinos [43, 44, 45, 46, 47]. (iii) The $\tau_{\widetilde{\tau}_1}$ limit can point to a CMSSM mass spectrum which will be difficult to probe at the Large Hadron Collider (LHC) [48, 40, 41, 42]. Indeed, the $\tau_{\widetilde{\tau}_1}$ limit can be relaxed only with a significant reduction of (1.1) which has been presented explicitly so far only for non-standard cosmological scenarios with a very low value of $T_{\rm R}$ [49] or with late-time entropy production after $\widetilde{\tau}_1$ decoupling and before BBN [40, 50].[2]

In this work we calculate the decoupling of the lighter stau from the primordial plasma by taking into account the complete set of stau annihilation channels in the MSSM with real parameters for SUSY spectra for which sparticle coannihilation is negligible. Using our own code for the computation of the resulting thermal relic stau abundance $Y_{\widetilde{\tau}}$, we examine explicitly (i) the effect of left–right mixing of the lighter stau, (ii) the effect of large stau–Higgs couplings, and (iii) stau annihilation at the resonance of the heavy CP-even Higgs boson H^0. We consider both the "phenomenological MSSM" (pMSSM) (see, e.g., [51]) in which the soft SUSY breaking parameters can be set at the weak scale, and the CMSSM, in which the gaugino masses, the scalar masses, and the trilinear scalar couplings are assumed to take on the respective universal values $m_{1/2}$, m_0, and A_0 at the scale of grand unification $M_{\rm GUT} \simeq 2 \times 10^{16}$ GeV. Within the framework of the pMSSM, we show examples in which $Y_{\widetilde{\tau}}$ can be well below 10^{-15}. Even within the CMSSM, we encounter regions with exceptionally small values of $Y_{\widetilde{\tau}} \lesssim 2 \times 10^{-15}$. The implications of these findings are discussed for scenarios with the gravitino LSP and the stau NLSP. We also address the viability of a $\widetilde{\tau}_1$–$\widetilde{\tau}_1^*$ asymmetry. Remarkably, we find that key quantities for the significant $Y_{\widetilde{\tau}}$ reduction could be probed at both the LHC and the International Linear Collider (ILC).

A calculation of the thermal relic abundance of long-lived staus has also been part of a recent thorough study [52] which focusses on gauge interactions and on the effect of Sommerfeld enhancement. In contrast, the most striking findings of our study—in which Sommerfeld enhancement is not taken into account—are related to the Higgs sector of the MSSM. At this point, we should also stress that the `micrOMEGAs` code [53, 54, 55, 56] allows for sophisticated calculations of the thermal relic stau abundance also in regions in which coannihilation effects become important. In fact, `micrOMEGAs` has already been applied in several studies to calculate $Y_{\widetilde{\tau}}$ [38, 40, 57, 42, 52]. In this paper, we also work with `micrOMEGAs` to cross check the results of our own $Y_{\widetilde{\tau}}$ calculation and to calculate $Y_{\widetilde{\tau}}$ in parameter regions in which sparticle coannihilations become relevant.

The outline of this paper is as follows. In the next section we review basic properties of the staus to introduce our notations and conventions for the stau mixing angle. Sec-

[2] Note that some implications of the $\tau_{\widetilde{\tau}_1}$ limit can be evaded not only by relaxing it but also by respecting it, e.g., R-parity violation can lead to $\tau_{\widetilde{\tau}_1} < 5 \times 10^3$ s [11].

tion 3 explains the way in which we calculate $Y_{\widetilde{\tau}}$ and provides the complete list of stau annihilation channels. In Sect. 4 we analyze the dependence of the most relevant stau annihilation channels on the stau mixing angle. Effects of large stau–Higgs couplings and stau annihilation at the H^0 resonance are studied in Sects. 5 and 6, respectively. The viability of a $\widetilde{\tau}_1$–$\widetilde{\tau}_1^*$ asymmetry is addressed in Sect. 7. In Sect. 8 we present exemplary parameter scans within the CMSSM that exhibit exceptionally small $Y_{\widetilde{\tau}}$ values. Potential collider phenomenology of the parameter regions associated with those exceptional relic abundances and potential implications for gravitino dark matter scenarios are discussed in Sects. 9 and 10, respectively.

2. Stau mixing and mass eigenstates

In this section we review some basic properties of the stau to set the notation. In absence of inter-generational mixing, the stau mass-squared matrix in the basis of the gauge eigenstates $(\widetilde{\tau}_\mathrm{L}, \widetilde{\tau}_\mathrm{R})$ reads

$$\mathcal{M}^2_{\widetilde{\tau}} = \begin{pmatrix} m_\tau^2 + m^2_\mathrm{LL} & m_\tau X_\tau^* \\ m_\tau X_\tau & m_\tau^2 + m^2_\mathrm{RR} \end{pmatrix} = (R_{\widetilde{\tau}})^\dagger \begin{pmatrix} m^2_{\widetilde{\tau}_1} & 0 \\ 0 & m^2_{\widetilde{\tau}_2} \end{pmatrix} R_{\widetilde{\tau}} \tag{2.1}$$

with

$$m^2_\mathrm{LL} = m^2_{\widetilde{\tau}_\mathrm{L}} + \left(-\frac{1}{2} + \sin^2\theta_W\right) M_\mathrm{Z}^2 \cos 2\beta \tag{2.2}$$

$$m^2_\mathrm{RR} = m^2_{\widetilde{\tau}_\mathrm{R}} - \sin^2\theta_W M_\mathrm{Z}^2 \cos 2\beta \tag{2.3}$$

$$X_\tau = A_\tau - \mu^* \tan\beta \ . \tag{2.4}$$

Here, $m_{\widetilde{\tau}_\mathrm{L}}$ and $m_{\widetilde{\tau}_\mathrm{R}}$ are the soft SUSY breaking masses, A_τ is the trilinear coupling, μ is the Higgs-higgsino mass parameter, and $\tan\beta = v_2/v_1$ denotes the ratio of the two Higgs vacuum expectation values. In this work we restrict ourselves to the MSSM with real parameters. Then $X_\tau^* = X_\tau$ so that the mass eigenstates $\widetilde{\tau}_1$ and $\widetilde{\tau}_2$ are related to $\widetilde{\tau}_\mathrm{L}$ and $\widetilde{\tau}_\mathrm{R}$ by means of an orthogonal transformation

$$\begin{pmatrix} \widetilde{\tau}_1 \\ \widetilde{\tau}_2 \end{pmatrix} = R_{\widetilde{\tau}} \begin{pmatrix} \widetilde{\tau}_\mathrm{L} \\ \widetilde{\tau}_\mathrm{R} \end{pmatrix} \quad \text{with} \quad R_{\widetilde{\tau}} = \begin{pmatrix} \cos\theta_{\widetilde{\tau}} & \sin\theta_{\widetilde{\tau}} \\ -\sin\theta_{\widetilde{\tau}} & \cos\theta_{\widetilde{\tau}} \end{pmatrix} \tag{2.5}$$

with $\theta_{\widetilde{\tau}}$ denoting the stau mixing angle. Imposing the mass ordering $m_{\widetilde{\tau}_1} < m_{\widetilde{\tau}_2}$ and choosing $0 \leq \theta_{\widetilde{\tau}} < \pi$, the mixing angle can be inferred from the elements of $\mathcal{M}^2_{\widetilde{\tau}}$,

$$\tan 2\theta_{\widetilde{\tau}} = \frac{2 m_\tau X_\tau}{m^2_\mathrm{LL} - m^2_\mathrm{RR}} = \frac{2 m_\tau X_\tau}{\delta} \ , \qquad \sin 2\theta_{\widetilde{\tau}} = \frac{2 m_\tau X_\tau}{m^2_{\widetilde{\tau}_1} - m^2_{\widetilde{\tau}_2}} \ , \tag{2.6}$$

where the sign of the second relation determines the quadrant of $\theta_{\widetilde{\tau}}$. In the first relation, we have introduced $\delta \equiv m^2_\mathrm{LL} - m^2_\mathrm{RR}$. In particular, $\theta_{\widetilde{\tau}} = \pi/2$ corresponds to a purely right-handed stau, $\widetilde{\tau}_1 = \widetilde{\tau}_\mathrm{R}$, whereas maximal mixing occurs for $\theta_{\widetilde{\tau}} = \pi/4$ and $3\pi/4$. The physical stau masses are then given by

$$m^2_{\widetilde{\tau}_{1,2}} = m_\tau^2 + m^2_\mathrm{RR} + \frac{1}{2}\left[\delta \mp \sqrt{\delta^2 + 4 m_\tau^2 X_\tau^2}\right] \tag{2.7}$$

from which we see that an increase of $|X_\tau|$ leads to a reduction of $m_{\widetilde{\tau}_1}$.

3. Calculation of the thermal relic stau abundance

We have undertaken the effort to set up our own full-fledged relic abundance calculation. Let us in the following give a description of our approach to compute the stau yield $Y_{\widetilde{\tau}}$. Throughout this work we assume a standard cosmological history with a temperature T of the primordial plasma above the stau decoupling temperature $T_{\rm f}$ so that the lighter stau $\widetilde{\tau}_1$ was once in thermal equilibrium. Then, the total stau yield $Y_{\widetilde{\tau}} \equiv Y_{\widetilde{\tau}_1} + Y_{\widetilde{\tau}_1^*}$ is found by solving the well-known Boltzmann equation

$$\frac{dY_{\widetilde{\tau}}}{dt} = -s\langle\boldsymbol{\sigma} v\rangle \left[Y_{\widetilde{\tau}}^2 - (Y_{\widetilde{\tau}}^{\rm eq})^2\right] \ . \tag{3.1}$$

Using the Maxwell–Boltzmann approximation, the stau equilibrium yield $Y_{\widetilde{\tau}}^{\rm eq}$ is given by

$$Y_{\widetilde{\tau}}^{\rm eq} = \frac{m_{\widetilde{\tau}_1}^2 T}{\pi^2 s} K_2\left(\frac{m_{\widetilde{\tau}_1}}{T}\right) \tag{3.2}$$

and the thermally averaged annihilation cross section by [58]

$$\langle\boldsymbol{\sigma} v\rangle(T) = \frac{1}{2m_{\widetilde{\tau}_1}^4 T[K_2(m_{\widetilde{\tau}_1}/T)]^2} \int_{4m_{\widetilde{\tau}_1}^2}^{\infty} ds\, \sqrt{s} K_1\left(\frac{\sqrt{s}}{T}\right) P_{\rm eff}^2 \boldsymbol{\sigma}(s)\,, \tag{3.3}$$

where K_i is the modified Bessel function of order i and $P_{\rm eff} = \sqrt{s - 4m_{\widetilde{\tau}_1}^2}\Big/2$.

Note that $\langle\boldsymbol{\sigma} v\rangle$ contains all the information from the particle physics side. It is obtained by computing the total stau-annihilation cross section,

$$\boldsymbol{\sigma} \equiv \frac{1}{2}\,\sigma_{\rm tot} \quad \text{with} \quad \sigma_{\rm tot} = \sigma_{\widetilde{\tau}_1\,\widetilde{\tau}_1 \to \tau\tau} + \sum_X \sigma_{\widetilde{\tau}_1\,\widetilde{\tau}_1^* \to X} \ , \tag{3.4}$$

where the sum for the annihilation of $\widetilde{\tau}_1\,\widetilde{\tau}_1^*$ pairs[3] has to be taken over all final states X. The factor $1/2$ is convention but gives (3.1) its familiar form. The complete list of annihilation processes in the MSSM with real parameters—save for coannihilation processes—is given in Table 1.[4] In addition, this table shows all possible particle exchanges, where s, t, and u are the Mandelstam variables which denote the respective channel. A number of annihilation processes proceeds also via a four-point vertex. Those are marked in the column named "contact." Already by mere optical inspection, we immediately see that the Higgs sector plays potentially an important role in the determination of the stau yield $Y_{\widetilde{\tau}}$.

For all channels in Table 1, we generate `Fortran` code for the squared matrix elements $|\mathcal{M}_i|^2$ by using the computer algebra packages `FeynArts 5.4` [60, 61] and `FormCalc 5.3` [62, 63]. For a chosen point in the SUSY parameter space, we then compute the radiatively corrected superparticle spectrum by running the spectrum generator `SuSpect 2.40` [51]. Its output allows us to set all SUSY parameters so that we can compute the total cross

[3]Counting wise we distinguish between $\widetilde{\tau}_1\,\widetilde{\tau}_1^* \to X$ and the conjugate process $\widetilde{\tau}_1^*\,\widetilde{\tau}_1 \to \overline{X}$. In absence of CP violation in the SUSY sector, their cross sections agree so that we can solve a single Boltzmann equation (3.1) for obtaining $Y_{\widetilde{\tau}}$.

[4]For a purely right-handed stau $\widetilde{\tau}_1 = \widetilde{\tau}_{\rm R}$, the stau annihilation channels and associated cross sections have already been presented in Ref. [59] in the context of $\widetilde{\chi}_1^0$-$\widetilde{\tau}_1$ coannihilation.

Table 1: The complete set of stau annihilation channels in the MSSM with real parameters for scenarios in which sparticle coannihilations are negligible. The mass eigenstates of the Higgs fields are denoted by h^0, H^0, A^0, and $H^\pm$ and the ones of the neutralinos, the charginos, and the tau sneutrino by $\widetilde{\chi}^0_{1,..,4}$, $\widetilde{\chi}^\pm_{1,2}$, and $\widetilde{\nu}_\tau$, respectively. Because of the absence of a $\widetilde{\tau}_1\widetilde{\tau}_1 A^0$ coupling (cf. Sect. 5), s-channel exchange of the CP-odd Higgs boson A^0 and also $\widetilde{\tau}_1\widetilde{\tau}_1^* \to \gamma A^0$ do not appear.

$\widetilde{\tau}_1^{(*)}\,\widetilde{\tau}_1^{(*)} \to$	final state	s-channel	$t(u)$-channel	contact
	$\tau\tau$ $(\overline{\tau\tau})$	—	$\widetilde{\chi}^0_{1,..,4}$	—
$\widetilde{\tau}_1\widetilde{\tau}_1^* \to$	final state $X^\dagger$	s-channel	$t(u)$-channel	contact
	$\mu\overline{\mu}$, $e\overline{e}$	h^0, H^0, γ, Z	—	—
	$\tau\overline{\tau}$	h^0, H^0, γ, Z	$\widetilde{\chi}^0_{1,..,4}$	—
	$\nu_e\overline{\nu}_e$, $\nu_\mu\overline{\nu}_\mu$	Z	—	—
	$\nu_\tau\overline{\nu}_\tau$	Z	$\widetilde{\chi}^\pm_{1,2}$	—
	$q_k\overline{q}_k$	h^0, H^0, γ, Z	—	—
	$\gamma\gamma$, γZ	—	$\widetilde{\tau}_1$	✓
	ZZ	h^0, H^0	$\widetilde{\tau}_{1,2}$	✓
	W^+W^-	h^0, H^0, γ, Z	$\widetilde{\nu}_\tau$	✓
	γh^0, γH^0	—	$\widetilde{\tau}_1$	—
	Zh^0, ZH^0	Z	$\widetilde{\tau}_{1,2}$	—
	ZA^0	h^0, H^0	$\widetilde{\tau}_2$	—
	$W^\mp H^\pm$	h^0, H^0	$\widetilde{\nu}_\tau$	—
	h^0h^0, h^0H^0, H^0H^0	h^0, H^0	$\widetilde{\tau}_{1,2}$	✓
	A^0A^0	h^0, H^0	$\widetilde{\tau}_2$	✓
	h^0A^0, H^0A^0	Z	$\widetilde{\tau}_2$	—
	H^+H^-	h^0, H^0, γ, Z	$\widetilde{\nu}_\tau$	✓

† $k = u,\, d,\, c,\, s,\, t,\, b$

section $\sigma_{\rm tot}(s)$ given by (3.4) and subsequently the thermally averaged cross section (3.3). Numerically, the computation of (3.3) is the most demanding part in the relic abundance calculation. In particular, we take special care about the following cases:

- H^0-resonance: Resonant stau annihilation via H^0 exchange is one of the central points in this paper. In the generation of the matrix elements, we have therefore included the total H^0-width Γ_{H^0} in the respective s-channel propagators.

- Propagator poles: A diverging $t(u)$-channel propagator can be encountered when a

production threshold is met. We overcome this problem by including a "sparticle-width" of $0.01 m_{\widetilde{\tau}_1}$ in the respective propagators in the vicinity of dangerous thresholds. A particularly interesting example with a diverging $t(u)$-channel propagator is given by the process $\widetilde{\tau}_1 \widetilde{\tau}_1^* \to \gamma H^0$ if $\sqrt{s} = m_{H^0}$ is fulfilled since then the H^0-exchange in the s-channels of other processes is resonant simultaneously.

- Bessel functions: The Bessel functions in (3.2) and (3.3) exhibit an exponential behavior for large arguments $x \gg 1$ [64]

$$K_n(x) \simeq \sqrt{\frac{\pi}{2\,x}} e^{-x} \left(1 + \frac{4n^2 - 1}{8x} + \dots\right) . \tag{3.5}$$

  For small temperatures T, the arguments of K_1 and K_2 in (3.3) become large simultaneously. Therefore, in order to ensure numerical stability, we expand the Bessel functions in (3.3) for $m_{\widetilde{\tau}_1}/T > 35$ as in (3.5) and cancel the exponents analytically.[5]

We find the starting point for the numerical integration of (3.1) by solving [54]

$$\left.\frac{dY_{\widetilde{\tau}}^{\rm eq}}{dT}\right|_{T_{\rm f1}} = \sqrt{\frac{8\pi^2 g_*(T)}{45}} \mathrm{M_P} \langle \boldsymbol{\sigma} v \rangle (Y_{\widetilde{\tau}}^{\rm eq})^2 \lambda(\lambda + 2) \tag{3.6}$$

where $g_*(T)$ is a degrees of freedom parameter [58] and $\mathrm{M_P} = 2.4 \times 10^{18}$ GeV the (reduced) Planck mass. $T_{\rm f1}$ marks the point at which the stau starts to decouple chemically from the background plasma, $Y_{\widetilde{\tau}}(T_{\rm f1}) - Y_{\widetilde{\tau}}^{\rm eq}(T_{\rm f1}) \simeq \lambda Y_{\widetilde{\tau}}^{\rm eq}(T_{\rm f1})$ with $\lambda = 0.1$ [54] chosen in our code. Since we use a globally adaptive Gaussian integration routine to calculate (3.3), the computation of $\langle \boldsymbol{\sigma} v \rangle(T)$ is time-demanding. Therefore, we evaluate (3.3) on a grid of different temperatures and use cubic spline interpolation to obtain values in between. We then solve the Boltzmann equation (3.1) by numerical integration from $T_{\rm f1}$ to zero. There, we fully take into the account the temperature dependence of g_* and g_{*S} by interpolating the respective tabulated values provided as part of the relic density code `DarkSUSY 4.00` [65]. The freeze out temperature can then be defined by $T_{\rm f} \equiv (T_{\rm f1} + T_{\rm f2})/2$ where $T_{\rm f2}$ is given by $Y_{\widetilde{\tau}}^{\rm eq}(T_{\rm f2}) = Y_{\widetilde{\tau}}(T_{\rm f2})/10$ [54]. For $T < T_{\rm f2}$, residual annihilations will further reduce $Y_{\widetilde{\tau}}$ so that we refer to the decoupling yield $Y_{\widetilde{\tau}}^{\rm dec}$ as the quantity at the endpoint of integration. For simplicity, we call this yield $Y_{\widetilde{\tau}}$ in the Introduction and in the following. Moreover, we will quantify T in terms of $x \equiv m_{\widetilde{\tau}_1}/T$ and in particular $T_{\rm f}$ in terms of $x_{\rm f} \equiv m_{\widetilde{\tau}_1}/T_{\rm f}$.

Note that we have additionally modified the `FeynArts` MSSM model file for the generation of the matrix elements in two ways: The first version, which we use throughout Sects. 4–6, allows us to set all $q_k \overline{q}_k$–Higgs and all trilinear Higgs couplings by using the computer tool `FeynHiggs 2.6.3` [66]; see also Sects. 5 and 6. The second version allows for a direct comparison with the existing computer code `micrOMEGAs 2.0.6` [53, 54, 67]. We have transcribed their routine [68] for the computation of the running quark masses to `Fortran`, adopted all $q_k \overline{q}_k$–Higgs couplings, and modified all Higgs-self couplings of our

[5] J.P. is grateful to P. Gondolo and J. Edsjo for pointing out that trick.

matrix elements to match with their implemented version of the MSSM [69]. Using this second version, we find perfect agreement between our codes.[6]

4. Dependence of stau annihilation on the stau mixing angle

In order to isolate the distinct features of the different annihilation processes we need to have full control over the superparticle mass spectrum. Therefore, in the following, we will not rely on any constrained model (such as the CMSSM) where the soft-SUSY breaking parameters are subject to stringent boundary conditions at some high scale (such as $M_{\rm GUT}$). In those models, the mass spectrum is found only after renormalization group (RG) evolution from the high scale down to the electroweak scale. Instead, we choose to work in the framework of the "phenomenological MSSM" (pMSSM), see, e.g., [51]. There, all soft-SUSY breaking parameters can be set at the scale of electroweak symmetry breaking—a low scale—which we fix to $\sim 2m_{\widetilde{\tau}_1}$. In particular, one can also trade the Higgs mass-squared parameters $m^2_{H_u}$ and $m^2_{H_d}$ against μ and the pseudoscalar Higgs boson mass m_{A^0}.[7] Choosing μ as an input parameter is very convenient for two reasons: First, together with the specification of the gaugino masses $M_{1,2}$ we have control over the gaugino/higgsino mixture of the neutralinos $\widetilde{\chi}^0_i$. Second, μ enters directly into the stau-Higgs couplings, whose importance will become clear in the next section. Furthermore, in the following, we choose to set all soft-SUSY breaking scalar masses (apart from $m_{\widetilde{\tau}_{\rm L}}$ and $m_{\widetilde{\tau}_{\rm R}}$) to a common value $M_S = 1$ TeV. Thereby, we essentially decouple all sfermions which are not of interest for us. This ensures also that we never enter *accidentally* any coannihilation regime. Finally, for simplicity, we set also all trilinear parameters to a common value A. Given μ, $A_\tau = A$, and $\tan\beta$, and thereby X_τ, we can then fix $m_{\widetilde{\tau}_1}$ and $\theta_{\widetilde{\tau}}$ to arbitrary values by adjusting $m^2_{\rm RR}$ and δ in Eqs. (2.6) and (2.7).

In the following, we will focus on two distinct regions of the SUSY parameter space. In the beginning, we will choose m_{A^0} to be very large $m_{A^0} = 1$ TeV $\gg M_{\rm Z}$. This corresponds to the decoupling limit of the MSSM where the following (tree-level) relations hold [70]

$$m^2_{h^0} \simeq M^2_{\rm Z}\cos^2 2\beta, \qquad m^2_{H^0} \simeq m^2_{A^0} + M^2_{\rm Z}\sin^2 2\beta, \tag{4.1}$$

$$m^2_{\rm H^\pm} = m^2_{A^0} + M^2_{\rm W}, \qquad \cos^2(\beta-\alpha) \simeq \frac{M^4_{\rm Z}\sin^2 4\beta}{4m^4_{A^0}}. \tag{4.2}$$

Therefore, $m_{A^0} \simeq m_{H^0} \simeq m_{\rm H^\pm}$ up to corrections $\mathcal{O}\left(M^2_{\rm Z}/m_{A^0}\right)$ so that any of the stau annihilation channels into heavy Higgs bosons is kinematically blocked. Furthermore, $\cos(\beta-\alpha) = 0$ up to corrections $\mathcal{O}\left(M^2_{\rm Z}/m^2_{A^0}\right)$ implies that the H^0VV coupling ($V = Z, W$) becomes very small so that we loose the H^0-exchanges in the stau annihilation

[6] For our computation we use the Standard Model parameters $m_{\rm t} = 172.5$ GeV, $m_{\rm b}(m_{\rm b})^{\overline{\rm MS}} = 4.25$ GeV, $\alpha_{\rm s}^{\overline{\rm MS}}(M_{\rm Z}) = 0.1172$, $\alpha_{\rm em}^{-1\overline{\rm MS}}(M_{\rm Z}) = 127.932$, and $M_{\rm Z} = 91.187$ GeV. Since `micrOMEGAs` has hard-coded $\sin\theta_W = 0.481$ from which it computes $M_{\rm W}$ using the on-shell relation with $M_{\rm Z}$, we follow their convention to allow for a better comparison of our results with `micrOMEGAs`.

[7] Though the advocated procedure may require fine-tuning in the electroweak symmetry breaking conditions, it conveniently provides us with running parameters at the scale of stau annihilation.

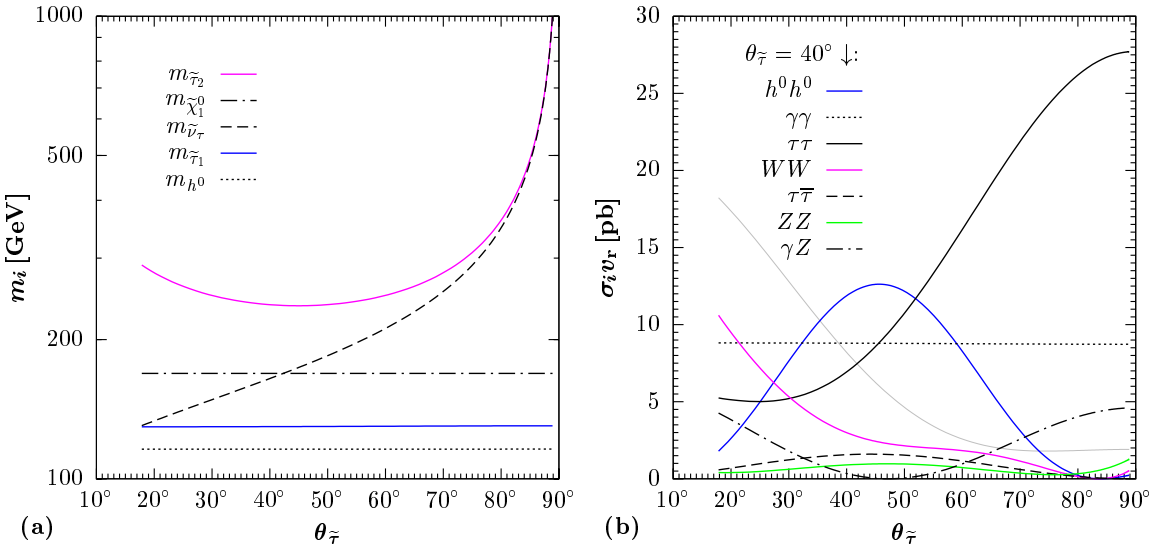

Figure 1: (a) The dependence of $m_{\tilde{\tau}_2}$ (curved solid line) and $m_{\tilde{\nu}_\tau}$ (dashed line) on the stau mixing angle $\theta_{\tilde{\tau}}$ for the input parameters $m_{\tilde{\tau}_1} = 130$ GeV (horizontal solid line), $\tan\beta = 10$, $m_{A^0} = M_S = M_3 = -A = 1$ TeV, and $6M_1 = M_2 = \mu = 1$ TeV (i.e., $\widetilde{\chi}_1^0 \simeq \widetilde{B}$) for which $m_{\widetilde{\chi}_1^0} = 169$ GeV (dash-dotted line) and $m_{h^0} = 116$ GeV (dotted line). (b) Dominant stau annihilation cross sections times the relative velocity $v_{\rm r}$ of the incoming staus as a function of $\theta_{\tilde{\tau}}$ for $P_{\rm eff} = 10$ GeV and the same input parameters as in (a). The curves show the channels with the following final states: h^0h^0, $\gamma\gamma$, $\tau\tau$, WW, $\tau\overline{\tau}$, ZZ, γZ (at $\theta_{\tilde{\tau}} = 40°$, from top to bottom). In addition, we plot $\sigma_{\tau\tau}v_{\rm r}$ for the case of a wino-like neutralino, $\widetilde{\chi}_1^0 \simeq \widetilde{W}$, with $m_{\widetilde{\chi}_1^0} = 175$ GeV as obtained with $M_1 = 6M_2 = 1$ TeV (thin gray line). No lines are shown for $\theta_{\tilde{\tau}} < 18°$ where $m_{\tilde{\nu}_\tau} < m_{\tilde{\tau}_1}$.

channels with a VV final state. At the same time, the light Higgs boson takes on its Standard Model value for the h^0VV coupling. Complementary to that we will consider also regions of the SUSY parameter space with smaller m_{A^0}, e.g., in the next section, where we will put a stronger focus on the Higgs sector and its connection to $Y_{\tilde{\tau}}$.

In Fig. 1a we show the $\theta_{\tilde{\tau}}$-dependence of the masses of the heavier stau, $m_{\tilde{\tau}_2}$, (curved solid line) and the tau-sneutrino, $m_{\tilde{\nu}_\tau}$, (dashed line) for fixed $m_{\tilde{\tau}_1} = 130$ GeV and the input parameters $\tan\beta = 10$, $m_{A^0} = \mu = -A = 1$ TeV, and $6M_1 = M_{2,3} = 1$ TeV. Because of SU(2) gauge invariance, $m_{\tilde{\tau}_{\rm L}}$ sets also the soft-breaking mass for the tau-sneutrino hence approximately $m^2_{\tilde{\nu}_\tau} \sim m^2_{\tilde{\tau}_{\rm R}} + \delta$ so that $\widetilde{\nu}_\tau$ becomes lighter than $\widetilde{\tau}_1$ for $\theta_{\tilde{\tau}} \lesssim 18°$ (δ is negative in that region). In addition, we plot the masses of the lightest neutralino, $m_{\widetilde{\chi}_1^0} = 169$ GeV (dash-dotted line), the lighter stau, $m_{\tilde{\tau}_1} = 130$ GeV (horizontal solid line), and the lightest Higgs, $m_{h^0} = 116$ GeV (dotted line). We note in passing that $m_{\tilde{\tau}_1}$ may deviate slightly from its anticipated input value due to radiative corrections. We then correct for this by an adjustment of $m^2_{\tilde{\tau}_{\rm R}}$ so that we indeed ensure $m_{\tilde{\tau}_1}$ to be constant.

In Fig. 1b we plot the dominant stau annihilation cross sections times the relative (non-relativistic) velocity in the center-of-mass frame of the incoming staus, $v_{\rm r} = 2P_{\rm eff}/m_{\tilde{\tau}_1}$, for the same parameters as in Fig. 1a. Owing to an (approximate) Maxwell-Boltzmann distri-

bution of the stau velocity, $\langle P_{\rm eff}\rangle|_{T_{\rm f}} \sim \sqrt{m_{\widetilde{\tau}_1} T_{\rm f}}$, we choose $P_{\rm eff} = 10$ GeV as a representative value.[8] The curves show the annihilation channels with the following final states: h^0h^0, $\gamma\gamma$, $\tau\tau$, WW, $\tau\overline{\tau}$, ZZ, γZ (at $\theta_{\widetilde{\tau}} = 40°$, from top to bottom). All channels except $\gamma\gamma$ show a strong dependence on $\theta_{\widetilde{\tau}}$. The h^0h^0 ($\tau\overline{\tau}$) channel peaks at $\theta_{\widetilde{\tau}} = \pi/4$—a feature which we will discuss in detail in Sect. 5. For the $\tau\tau$ channel, the overall size of the cross section is governed by $m_{\widetilde{\chi}_1^0}$ since this channel proceeds only via $t(u)$-channel exchanges of neutralinos. Our chosen input values lead to a bino-like neutralino, $\widetilde{\chi}_1^0 \simeq \widetilde{B}$, and $\sigma_{\tau\tau}$ drops for an increasingly 'left-handed' stau. (For comparison, the thin gray line shows $\sigma_{\tau\tau}v_{\rm r}$ for the case of a wino-like lightest neutralino, $\widetilde{\chi}_1^0 = \widetilde{W}$, of similar mass, $m_{\widetilde{\chi}_1^0} = 175$ GeV, as obtained by changing the gaugino mass input parameters to $M_1 = 6M_2 = 1$ TeV.) The annihilation into a WW pair becomes important for an increasing $\widetilde{\tau}_{\rm L}$ component in $\widetilde{\tau}_1$, i.e., towards smaller $\theta_{\widetilde{\tau}}$, since the $t(u)$-channel exchange with the tau-sneutrino opens up; the $\widetilde{\tau}_1\widetilde{\nu}_\tau W$ ($\widetilde{\tau}_1\widetilde{\tau}_1 WW$) coupling is proportional to $\cos\theta_{\widetilde{\tau}}$ ($\cos^2\theta_{\widetilde{\tau}}$). The modulation of the γZ channel can be understood by considering the structure of the $\widetilde{\tau}_1\widetilde{\tau}_1 Z$ coupling $\propto (1 - 4\sin^2\theta_W + \cos 2\theta_{\widetilde{\tau}})$. Note that the first two terms practically cancel out. For stau annihilation into a ZZ pair there is an additional contribution from $\widetilde{\tau}_2$-exchange with the respective $\widetilde{\tau}_1\widetilde{\tau}_2 Z$ coupling $\propto \sin 2\theta_{\widetilde{\tau}}$. Having discussed the dominant $\widetilde{\tau}_1$ annihilation channels in a simple manner, we also warn the reader that interferences between the different Feynman diagrams of a given channel may well lead to a counterintuitive behavior. In this regard, see Ref. [52] for a thorough discussion of $\widetilde{\tau}_1\widetilde{\tau}_1^*$ annihilation into vector bosons. For the limiting case of a purely 'right-handed' stau, $\widetilde{\tau}_1 \simeq \widetilde{\tau}_{\rm R}$ ($\theta_{\widetilde{\tau}} \to \pi/2$), we recover the relative importance of the annihilation cross sections into $\gamma\gamma$, γZ, ZZ, and $\tau\tau$ with bino $t(u)$-channel exchange found in Ref. [37].

Figure 2 shows the $\theta_{\widetilde{\tau}}$-dependence of $Y_{\widetilde{\tau}}$ (upper panel) and of the relative importance of the dominant *thermally averaged* cross sections, $\langle\sigma_i v\rangle/\langle\sigma_{\rm tot}v\rangle$, at $x = 25$ (lower panel) for the same input parameters as in Fig. 1. The lines in the lower panel are associated with the same dominant annihilation channels as in Fig. 1b. In addition, the relative importance of the sum of the displayed cross sections, $\langle\sigma_{\rm disp}v\rangle/\langle\sigma_{\rm tot}v\rangle$, (thin line, as labeled) is shown to demonstrate that the displayed channels constitute indeed (up to at most about 10%) the dominant part of $\langle\sigma_{\rm tot}v\rangle$ for the chosen set of input parameters. In the upper panel, the total stau decoupling yield obtained with our own relic abundance calculation is shown by the thick line and the one computed with `micrOMEGAs`, $Y_{\widetilde{\tau}}^{\rm m\Omega}$, by the thin gray line. For $\theta_{\widetilde{\tau}} \lesssim 25°$, both curves start to deviate from each other since one enters the $\widetilde{\nu}_\tau$–$\widetilde{\tau}_1$ coannihilation region in which the stau decoupling yield increases. This coannihilation effect leads also to the rise of the thin gray line that shows $\langle\sigma_{\rm tot}v\rangle\, Y_{\widetilde{\tau}}^{\rm m\Omega}$ in arbitrary units (a.u.) in the lower panel. Note that the same line illustrates $Y_{\widetilde{\tau}} \propto 1/\langle\sigma_{\rm tot}v\rangle$ for $\theta_{\widetilde{\tau}} > 25°$, where the result of our relic abundance calculation agrees with $Y_{\widetilde{\tau}}^{\rm m\Omega}$. Interestingly, for the given input parameters, $Y_{\widetilde{\tau}}$ is not overly affected by the variation in $\theta_{\widetilde{\tau}}$ in this region, which reflects the fact that $\langle\sigma_{\rm tot}v\rangle$ and thereby $\langle\boldsymbol{\sigma}v\rangle$ vary by less than a factor of about 1.5 at the relevant time of decoupling. In the next sections, we will demonstrate that this picture

[8] This value is actually at the somewhat lower end, given $m_{\widetilde{\tau}_1} \gtrsim 100$ GeV and $T_{\rm f} \simeq m_{\widetilde{\tau}_1}/25$. However, $\sigma v_{\rm r}$ depends only weakly on $P_{\rm eff}$, and the thermally averaged $\langle\sigma_i v\rangle$ will be shown in the upcoming figures.

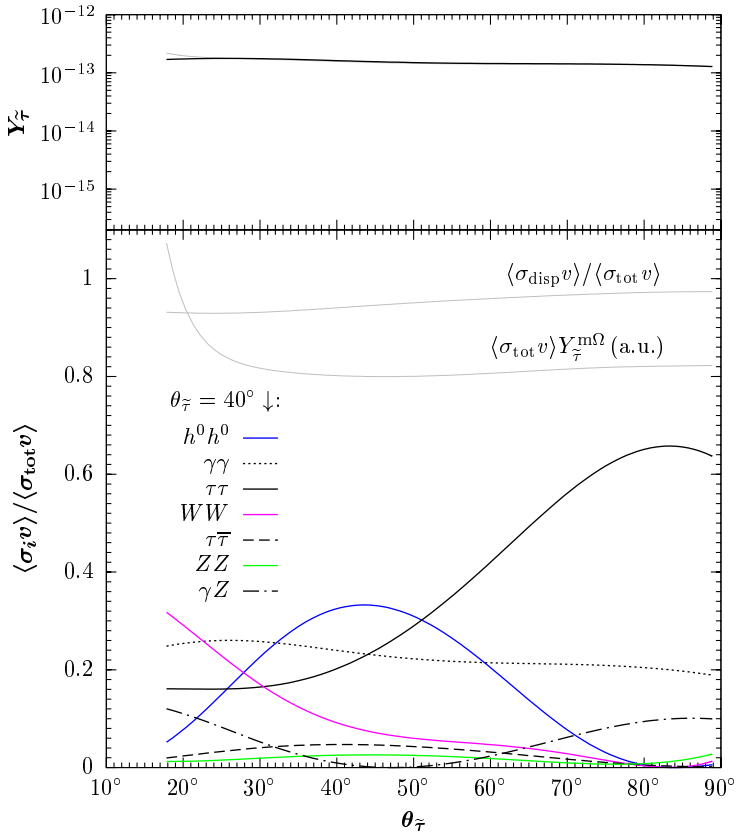

Figure 2: Dependence of the stau yield $Y_{\tilde{\tau}}$ (upper panel) and of the relative importance of the dominant thermally averaged cross sections, $\langle\sigma_i v\rangle/\langle\sigma_{\rm tot} v\rangle$, at $x = 25$ (lower panel) on the stau-mixing angle $\theta_{\tilde{\tau}}$ for the same input parameters as in Fig. 1. In the upper panel, the thick line shows the stau yield $Y_{\tilde{\tau}}$ obtained with our relic abundance calculation and the thin gray line the one obtained with `micrOMEGAs` to which we refer as $Y_{\tilde{\tau}}^{\rm m\Omega}$. In the lower panel, the line styles are associated with the same dominant annihilation channels as in Fig. 1b. In addition, we show (as labeled) the relative importance of the sum of the displayed cross sections, $\langle\sigma_{\rm disp} v\rangle/\langle\sigma_{\rm tot} v\rangle$, and $\langle\sigma_{\rm tot} v\rangle\, Y_{\tilde{\tau}}^{\rm m\Omega}$ in arbitrary units (a.u.). No lines are shown for $\theta_{\tilde{\tau}} < 18^\circ$ where $m_{\tilde{\nu}_\tau} < m_{\tilde{\tau}_1}$.

changes significantly for certain other choices of the input parameters.

5. Effects of large stau-Higgs couplings

Owing to the scalar nature of the stau, there exists a remarkable difference between the standard neutralino decoupling and the scenario in which the long-lived stau freezes out from the primordial plasma. For the neutralino LSP, the μ parameter enters into the annihilation cross sections only indirectly by influencing the gaugino/higgsino mixture of $\widetilde{\chi}_1^0$. This stands in strong contrast to the case in which a scalar particle is the lightest Standard Model superpartner: the sfermions couple directly to dimensionful parameters of the theory, namely, the trilinear couplings A and the Higgs-higgsino mass parameter μ. The corresponding operators in the MSSM Lagrangian always contain a Higgs field. In

particular, the stau–Higgs couplings are given by

$$\mathcal{L}_{\text{MSSM}} \ni \frac{g}{M_{\text{W}}} \sum_{\alpha,\beta=\text{L,R}} \widetilde{\tau}_\alpha^* \widetilde{C}[\widetilde{\tau}_\alpha^*, \widetilde{\tau}_\beta, \mathcal{H}] \widetilde{\tau}_\beta \mathcal{H} \tag{5.1}$$

with $\mathcal{H} = h^0$, H^0, A^0. We have pulled out the factor g/M_{W} so that the 'reduced' couplings $\widetilde{C}[\widetilde{\tau}_\alpha^*, \widetilde{\tau}_\beta, \mathcal{H}]$ among the gauge eigenstates $\widetilde{\tau}_{\text{L}}$ and $\widetilde{\tau}_{\text{R}}$ are given by [71]

$$\widetilde{C}[\widetilde{\tau}^*, \widetilde{\tau}, h^0] = \begin{pmatrix} \left(-\frac{1}{2} + s_W^2\right) M_{\text{Z}}^2 s_{\alpha+\beta} + m_\tau^2 \frac{s_\alpha}{c_\beta} & \frac{m_\tau}{2}\left(A_\tau \frac{s_\alpha}{c_\beta} + \mu \frac{c_\alpha}{c_\beta}\right) \\ \frac{m_\tau}{2}\left(A_\tau \frac{s_\alpha}{c_\beta} + \mu \frac{c_\alpha}{c_\beta}\right) & -s_W^2 M_{\text{Z}}^2 s_{\alpha+\beta} + m_\tau^2 \frac{s_\alpha}{c_\beta} \end{pmatrix} , \tag{5.2}$$

$$\widetilde{C}[\widetilde{\tau}^*, \widetilde{\tau}, A^0] = \begin{pmatrix} 0 & +i\frac{m_\tau}{2}\left(A_\tau \tan\beta + \mu\right) \\ -i\frac{m_\tau}{2}\left(A_\tau \tan\beta + \mu\right) & 0 \end{pmatrix} , \tag{5.3}$$

where $\widetilde{C}[\widetilde{\tau}^*, \widetilde{\tau}, H^0]$ can be obtained from (5.2) upon the replacement $\alpha \to \alpha - \pi/2$. Whenever convenient, we use the shorthand notation $s_W^2 = \sin^2\theta_W$, $c_\gamma = \cos\gamma$, and $s_\gamma = \sin\gamma$. The parameters A_τ and μ only appear off-diagonal and they are multiplied with the associated fermion mass, the tau mass m_τ.

Using $C = R_{\widetilde{\tau}} \widetilde{C} R_{\widetilde{\tau}}^\dagger$, one obtains the couplings of the mass eigenstates $\widetilde{\tau}_1$ and $\widetilde{\tau}_2$. In this regard, it is important to note that the coupling of the CP-odd Higgs boson to the lighter stau vanishes, $C[\widetilde{\tau}_1^*, \widetilde{\tau}_1, A^0] = 0$. Therefore, we have not listed the process $\widetilde{\tau}_1\widetilde{\tau}_1^* \to \gamma A^0$ in Table 1. By the same token, there is also no s-channel exchange of A^0 in any of the annihilation channels. Note that this statement remains valid even after the inclusion of radiative corrections: There is no induced mixing between $h^0(H^0)$ and A^0 in absence of CP-violating effects in the SUSY sector.

Let us now turn to the probably most interesting couplings in the context of $\widetilde{\tau}_1\widetilde{\tau}_1^*$ annihilation, namely, the ones of the lighter stau to h^0 and H^0. The 'reduced' $\widetilde{\tau}_1\widetilde{\tau}_1 h^0$ coupling reads

$$C[\widetilde{\tau}_1^*, \widetilde{\tau}_1, h^0] = \left(-\frac{1}{2} c_{\theta_{\widetilde{\tau}}}^2 + s_W^2 c_{2\theta_{\widetilde{\tau}}}\right) M_{\text{Z}}^2 s_{\alpha+\beta} + m_\tau^2 \frac{s_\alpha}{c_\beta} + \frac{m_\tau}{2}\left(A_\tau \frac{s_\alpha}{c_\beta} + \mu \frac{c_\alpha}{c_\beta}\right) s_{2\theta_{\widetilde{\tau}}} . \tag{5.4}$$

This is a complicated expression. However, if we choose m_{A^0} to be large, $m_{A^0} \gg M_{\text{Z}}$, we can simplify (5.4) by using $\cos(\beta - \alpha) = 0$ [cf. (4.2)],

$$C^{\text{DL}}[\widetilde{\tau}_1^*, \widetilde{\tau}_1, h^0] \simeq \left(\frac{1}{2} c_{\theta_{\widetilde{\tau}}}^2 - s_W^2 c_{2\theta_{\widetilde{\tau}}}\right) M_{\text{Z}}^2 c_{2\beta} - m_\tau^2 - \frac{m_\tau}{2} X_\tau s_{2\theta_{\widetilde{\tau}}} . \tag{5.5}$$

Thereby, we make an interesting observation: In the decoupling limit (DL), the $\widetilde{\tau}_1\widetilde{\tau}_1 h^0$ coupling becomes proportional to the left–right entry $m_\tau X_\tau$ of the stau mass-squared matrix (2.1) and to $s_{2\theta_{\widetilde{\tau}}}$. Therefore, it comes as no surprise that the $\widetilde{\tau}_1\widetilde{\tau}_1^*$ annihilation cross section into h^0h^0 peaks at $\theta_{\widetilde{\tau}} = \pi/4$—the point of maximal $\widetilde{\tau}_{\text{L}}$-$\widetilde{\tau}_{\text{R}}$ mixing—as can be seen, e.g., in Fig. 1b. Analogously, one finds that the $\widetilde{\tau}_1\widetilde{\tau}_1 H^0$ coupling is proportional to $(A_\tau \tan\beta + \mu)\, s_{2\theta_{\widetilde{\tau}}}$ in the decoupling limit. Complementary, the $\widetilde{\tau}_1\widetilde{\tau}_2 h^0/H^0$ couplings

exhibit in this limit the same combination of A, μ, and $\tan\beta$ as their $\widetilde{\tau}_1\widetilde{\tau}_1$ counterparts but those terms are now multiplied by $c_{2\theta_{\widetilde{\tau}}}$ instead of $s_{2\theta_{\widetilde{\tau}}}$.

After the above discussion, it is clear that there exists the possibility to enhance the total stau annihilation cross section $\sigma_{\rm tot}$—and thereby to decrease $Y_{\widetilde{\tau}} \propto 1/\langle\sigma_{\rm tot}v\rangle$—by choosing a proper combination of large A, μ, and $\tan\beta$. In the remainder of this section, we will explore this possibility for two exemplary pMSSM scenarios.

Before proceeding let us make some technical comments. Large values of the previously mentioned parameters may well lead to large radiative corrections.[9] In order to arrive at a proper loop-improved tree-level result, we re-evaluate the entire Higgs sector using `FeynHiggs`. In particular, we have modified our generated matrix elements in a way that allows us to set all trilinear Higgs couplings to their loop-corrected values.[10] Note that this goes well beyond a simple $\alpha \to \alpha_{\rm eff}$ prescription. Only then, we mostly find better agreement of our cross sections for stau annihilation into two Higgses with the ones computed by `micrOMEGAs`. The latter program uses `CalcHEP` [68] for the generation of the matrix elements. There, the trilinear Higgs self-couplings have been expressed in terms of m_{h^0}, m_{H^0}, and m_{A^0} which effectively reabsorbs a bulk of the radiative corrections [69]. We therefore think that we do slightly better whenever we encounter some disagreement between the mentioned cross sections. Though the overall effect on $Y_{\widetilde{\tau}}$ is typically small, it can be at the level of 20% (see below). Finally, it is well known that a large A parameter may lead to charge/color breaking minima (CCB) in the scalar MSSM potential; see, e.g., Ref. [73]. `SuSpect` performs some basic checks which we take into account to make sure that we do not violate the constraints associated with CCB. In any case, our pMSSM scenarios shall be regarded as toy models which allow us to extract important features of primordial stau annihilation in the most transparent way.

In Fig. 3 we demonstrate the effect associated with a large $\widetilde{\tau}_1\widetilde{\tau}_1h^0$ coupling by presenting the $\theta_{\widetilde{\tau}}$-dependence of $Y_{\widetilde{\tau}}$ (upper panel) and of the relative importance of the dominant *thermally averaged* cross sections, $\langle\sigma_i v\rangle/\langle\sigma_{\rm tot}v\rangle$, at $x = 30$ (lower panel) for the pMSSM scenario associated with $m_{\widetilde{\tau}_1} = 130$ GeV, $\tan\beta = 50$, $m_{A^0} = M_S = M_3 = -A = 1$ TeV, and $6M_1 = M_2 = \mu = 1$ TeV. In this scenario, m_{h^0} stays in the range $117 - 119$ GeV and the lightest neutralino is bino-like with a mass of $m_{\widetilde{\chi}_1^0} = 169$ GeV. Stau annihilation into heavy Higgses remains kinematically forbidden. The curves in the lower panel are associated with stau annihilation into h^0h^0, WW, $\tau\tau$, ZZ, $\gamma\gamma$, and γZ (at $\theta_{\widetilde{\tau}} = 80^\circ$, from top to bottom). As is evident, the annihilation into h^0h^0 is enhanced already well before $\theta_{\widetilde{\tau}} = \pi/4$. At the peak position, $\sigma_{h^0h^0}v_{\rm r} \simeq 8.8 \times 10^3$ pb for $P_{\rm eff} = 10$ GeV (no thermal average), which is still three orders of magnitude below the unitarity bound for inelastic s-wave annihilation, $\sigma_{\rm u}v_{\rm r} = 8\pi/(m_{\widetilde{\tau}_1}P_{\rm eff})$ [74, 52]. Also the cross sections for stau annihilation into WW and ZZ are strongly enhanced towards $\theta_{\widetilde{\tau}} = \pi/4$ since the s-channel contribution of $\widetilde{\tau}_1\widetilde{\tau}_1 \to h^{0*} \to VV$ becomes very important. At their respective peak positions, $\sigma_{WW}v_{\rm r} \simeq 250$ pb and $\sigma_{ZZ}v_{\rm r} \simeq 130$ pb for $P_{\rm eff} = 10$ GeV. (Because of the dominance of the h^0h^0 channel, the corresponding maxima do not show up in Fig. 3 where

[9] In this context, note that we introduce a large $m_{\rm t}$–$m_{\widetilde{\rm t}_{1,2}}$ splitting when choosing $M_S = 1$ TeV.

[10] We are grateful to T. Plehn and M. Rauch for providing us, for cross-checking, with their implementation of a `Fortran` routine which calculates the Higgs self-couplings using the effective potential approach [72].

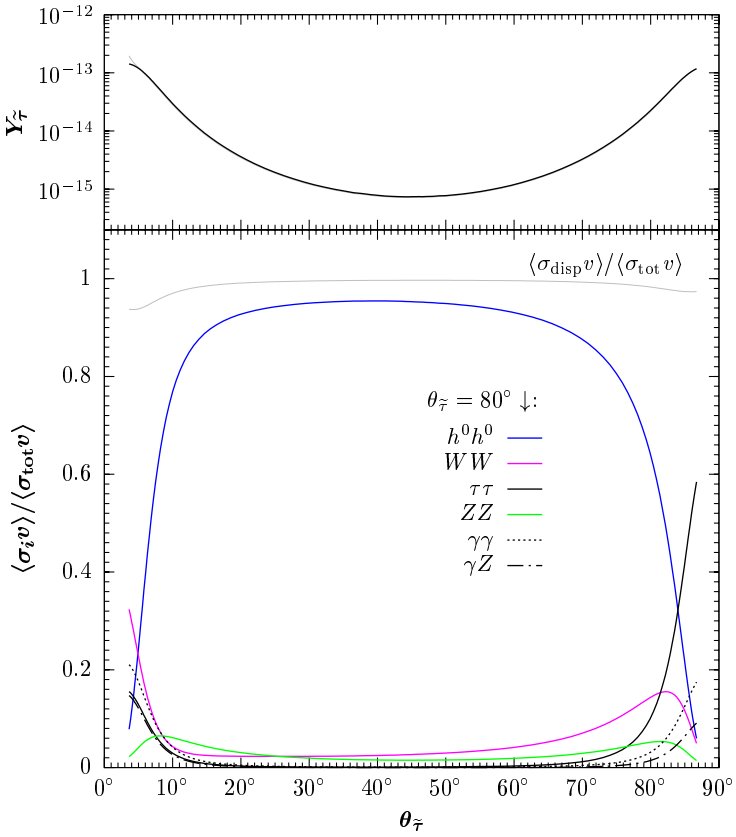

Figure 3: Analogous to Fig. 2 but for the pMSSM scenario associated with $m_{\tilde{\tau}_1} = 130$ GeV, $\tan\beta = 50$, and $m_{A^0} = \mu = M_S = 6M_1 = M_{2,3} = -A = 1$ TeV and for $x = 30$. The stau decoupling yield takes on its minimum value of $Y_{\tilde{\tau}} = 7.4 \times 10^{-16}$ at $\theta_{\tilde{\tau}} = 45°$. The displayed stau annihilation channels are associated with the following final states: h^0h^0, WW, $\tau\tau$, ZZ, $\gamma\gamma$, and γZ (at $\theta_{\tilde{\tau}} = 80°$, from top to bottom). No lines are shown for $\theta_{\tilde{\tau}} < 4°$ where $m_{\tilde{\nu}_\tau} < m_{\tilde{\tau}_1}$.

$\langle\sigma_i v\rangle/\langle\sigma_{\rm tot}v\rangle$ is shown.) By the same token, the cross sections of all (kinematically allowed) channels with a fermion-antifermion final state (e.g. $\tau\overline{\tau}$)—which are subdominant in the scenario considered in Fig. 3—experience an enhancement for $\theta_{\tilde{\tau}} \to \pi/4$. In total, there is an enhancement of $\langle\sigma_{\rm tot}v\rangle$ that delays the thermal freeze out of the staus significantly, i.e., $x_{\rm f} \simeq 33$ for $\theta_{\tilde{\tau}} \simeq \pi/4$. As can be seen in the upper panel of Fig. 3, the decoupling yield is thereby reduced dramatically down to a minimum value of $Y_{\tilde{\tau}} = 7.4 \times 10^{-16}$ for maximal left–right mixing of the staus.

In the previous pMSSM examples, annihilation into final states containing heavy Higgs bosons is kinematically forbidden. We can allow for those channels by reducing the input value m_{A^0}. Indeed, scenarios in which all Higgs bosons are very light in conjunction with large $\tan\beta$ have been studied in the literature, see, e.g., [75, 76] and references therein. We thus consider now the following pMSSM scenario: $m_{A^0} = 130$ GeV, $m_{\tilde{\tau}_1} = 150$ GeV, $\tan\beta = 50$, $M_S = M_3 = -A = 1$ TeV, and $3M_1 = M_2 = \mu = 1$ TeV. In Fig. 4, the associated $\theta_{\tilde{\tau}}$-dependence of $Y_{\tilde{\tau}}$ and of $\langle\sigma_i v\rangle/\langle\sigma_{\rm tot}v\rangle$ at $x = 30$ for the now dominant

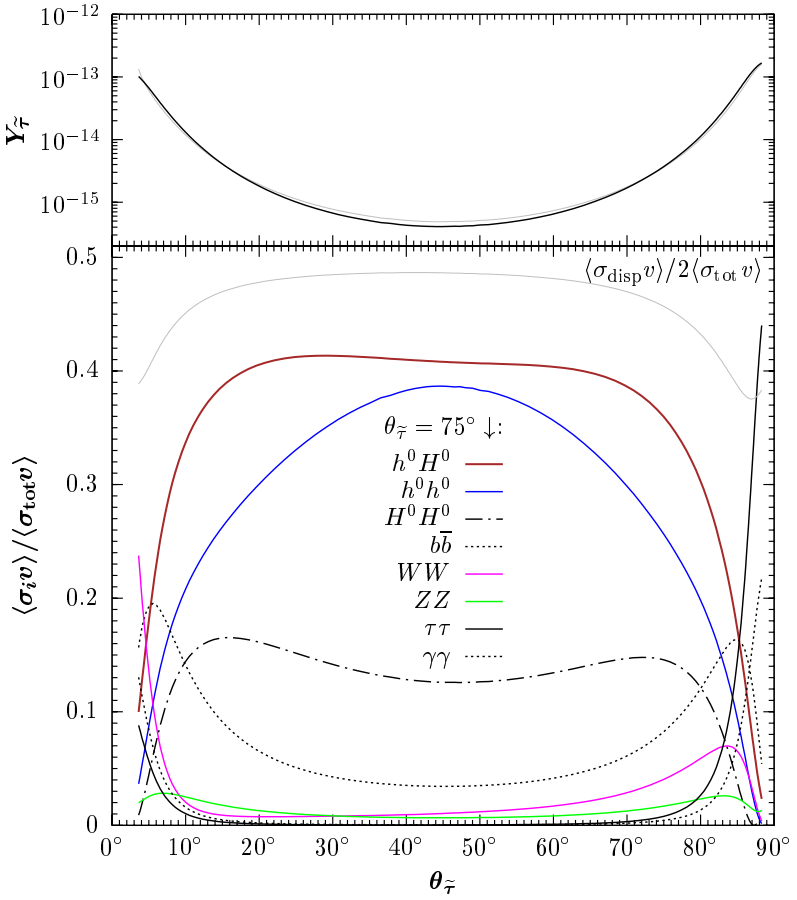

Figure 4: Analogous to Fig. 3 but for the pMSSM scenario associated with $m_{\tilde{\tau}_1} = 150$ GeV, $\tan\beta = 50$, $m_{A^0} = 130$ GeV, $M_S = M_3 = -A = 1$ TeV, $3M_1 = M_2 = \mu = 1$ TeV and for $x = 30$. The stau decoupling yield reaches its minimum value of $Y_{\tilde{\tau}} = 4.1\times10^{-16}$ at $\theta_{\tilde{\tau}} = \pi/4$. The displayed stau annihilation channels are associated with the following final states: h^0H^0, h^0h^0, H^0H^0, $b\overline{b}$, WW, ZZ, $\tau\tau$, and $\gamma\gamma$ (at $\theta_{\tilde{\tau}} = 75^\circ$, from top to bottom). For an optimized presentation of those channels, the line indicating the relative importance of the sum of the displayed cross sections is scaled down by a factor of 1/2: $\langle\sigma_{\rm disp}v\rangle/2\langle\sigma_{\rm tot}v\rangle$. No lines are shown for $\theta_{\tilde{\tau}} < 4^\circ$ where $m_{\tilde{\nu}_\tau} < m_{\tilde{\tau}_1}$.

channels is shown in a similar way as in Fig. 3; only the relative importance of the sum of the displayed cross sections is scaled down by a factor of 1/2, $\langle\sigma_{\rm disp}v\rangle/2\langle\sigma_{\rm tot}v\rangle$, to allow for an optimized presentation of the single dominant channels. Throughout the considered $\theta_{\tilde{\tau}}$ range, the masses of both CP-even Higgs bosons are relatively light and remain rather constant: $m_{h^0} = (118 \pm 1.5)$ GeV and $m_{H^0} = (128.5 \pm 1)$ GeV. Here the dominant annihilation channels are associated with the following final states: h^0H^0, h^0h^0, H^0H^0, $b\overline{b}$, WW, ZZ, $\tau\tau$, and $\gamma\gamma$ (at $\theta_{\tilde{\tau}} = 75^\circ$, from top to bottom). As can be seen, stau annihilation into h^0H^0 is now more dominant than the one into h^0h^0 and also the H^0H^0 channel becomes important, where each of those channels is indeed associated with an (absolute) annihilation cross section $\langle\sigma_i v\rangle$ that peaks at $\theta_{\tilde{\tau}} = \pi/4$. Also the annihilation into $b\overline{b}$ is significant—a process which we will discuss in detail in the following section.

In this respect, one should stress that all processes with s-channel H^0 exchange are here less suppressed by $m_{H^0}^2$ in the respective propagator than in the previously considered scenarios. Note that the asymmetry of $\langle\sigma_i v\rangle/\langle\sigma_{\rm tot} v\rangle$ of those dominant channels (h^0H^0, h^0h^0, H^0H^0, $b\overline{b}$) with respect to a reflection at $\theta_{\widetilde{\tau}} = \pi/4$ is dominantly caused by the $\theta_{\widetilde{\tau}}$-dependent modulation of the WW channel. As in the pMSSM scenario considered in Fig. 3, there is again an significant enhancement of $\langle\sigma_{\rm tot} v\rangle$ that delays the stau freeze out such that $x_{\rm f} \simeq 33$ at $\theta_{\widetilde{\tau}} \simeq \pi/4$. Thereby, the efficient annihilation into final state Higgses is accompanied by a significant drop in $Y_{\widetilde{\tau}}$ down to $Y_{\widetilde{\tau}} = 4.1 \times 10^{-16}$ at $\theta_{\widetilde{\tau}} = \pi/4$ as can be seen in Fig. 4. At this minimum, there is a 20% disagreement between $Y_{\widetilde{\tau}}$ from our calculation of stau decoupling (solid line) and the `micrOMEGAs` result $Y_{\widetilde{\tau}}^{\rm m\Omega}$ (thin gray line) which is a consequence of the different treatments of the Higgs sector described above.

Let us finally remark that the Higgs couplings to fermions and vector bosons as well as the Higgs self-couplings develop a strong dependence on m_{A^0} once we leave the decoupling regime ($m_{A^0} \lesssim 200$ GeV); for a comprehensive review see, e.g., Ref. [77].[11] Changes in m_{A^0} can therefore be accompanied by shifts in the relative importance of the corresponding annihilation cross sections. This underlines the fact that the details in the Higgs sector may very well be crucial for the determination of the relic abundance of a long-lived $\widetilde{\tau}_1$.

6. Resonant stau annihilation

By inspection of Table 1 it becomes clear that primordial stau annihilation can also proceed resonantly via s-channel exchange of the heavy CP-even Higgs boson H^0 for $m_{H^0} \simeq 2m_{\widetilde{\tau}_1}$. While the LEP bound on the stau mass $m_{\widetilde{\tau}_1} \gtrsim 82$ GeV [1] forbids h^0 to become on-shell ($m_{h^0}^{\rm max} \sim 140$ GeV, e.g., [77]), the s-channel exchange of A^0 is absent[12] because of $C[\widetilde{\tau}_1, \widetilde{\tau}_1^*, A^0] = 0$ (see Sect. 5). Again, our choice to work in the framework of the pMSSM proves to be very helpful. Since the H^0 resonance occurs for $2m_{\widetilde{\tau}_1} \simeq m_{H^0}$, one runs quickly into the decoupling limit in which m_{H^0} is governed by the input parameter m_{A^0} according to the simple relation (4.1). This allows us to scan through the resonance easily.

Let us explore resonant stau annihilation by considering the exemplary pMSSM scenario associated with $m_{\widetilde{\tau}_1} = 200$ GeV, $\theta_{\widetilde{\tau}} = 83°$ (i.e., a mostly 'right-handed' $\widetilde{\tau}_1$), $\tan\beta = 40$, and $-A = \mu = 4M_1 = M_{2,3} = M_S = 1$ TeV, for which we vary m_{A^0} (and thereby m_{H^0}) to scan through the resonance. Figure 5 shows the resulting m_{H^0}-dependence of $Y_{\widetilde{\tau}}$ (upper panel) and of $\langle\sigma_i v\rangle/\langle\sigma_{\rm tot} v\rangle$ at $x = 25$ for the dominant annihilation channels (lower panel). Those channels are now associated with the following final states: $b\overline{b}$, $\tau\tau$, $\tau\overline{\tau}$, $\gamma\gamma$, h^0h^0, WW, γZ, ZZ, and $t\overline{t}$ (at $m_{H^0} = 350$ GeV, from top to bottom). In Table 1 all resonant channels can be identified. Close to the resonance condition $2m_{\widetilde{\tau}_1} \simeq m_{H^0}$, the most important processes are stau annihilation into $b\overline{b}$ and $\tau\overline{\tau}$. This is because the couplings of those final state fermions to H^0 are $\tan\beta$ enhanced: for $\tan\beta \gg 1$, the $f\overline{f}H^0$ coupling

[11] The Higgs sector is also particularly sensitive to the mixing in the stop sector. In the considered pMSSM scenarios, $|X_t| \equiv |A_t - \mu\cot\beta| \sim M_S$ which corresponds to the "typical-mixing scenario" [78].

[12] Even in absence of SUSY-induced CP violation, resonant annihilation via A^0-exchange may still proceed through $\widetilde{\tau}_1$-$\widetilde{\tau}_2$ coannihilation. However, this scenario requires considerable fine-tuning in the stau mass-squared matrix since $\widetilde{\tau}_1$ and $\widetilde{\tau}_2$ have to be nearly degenerate.

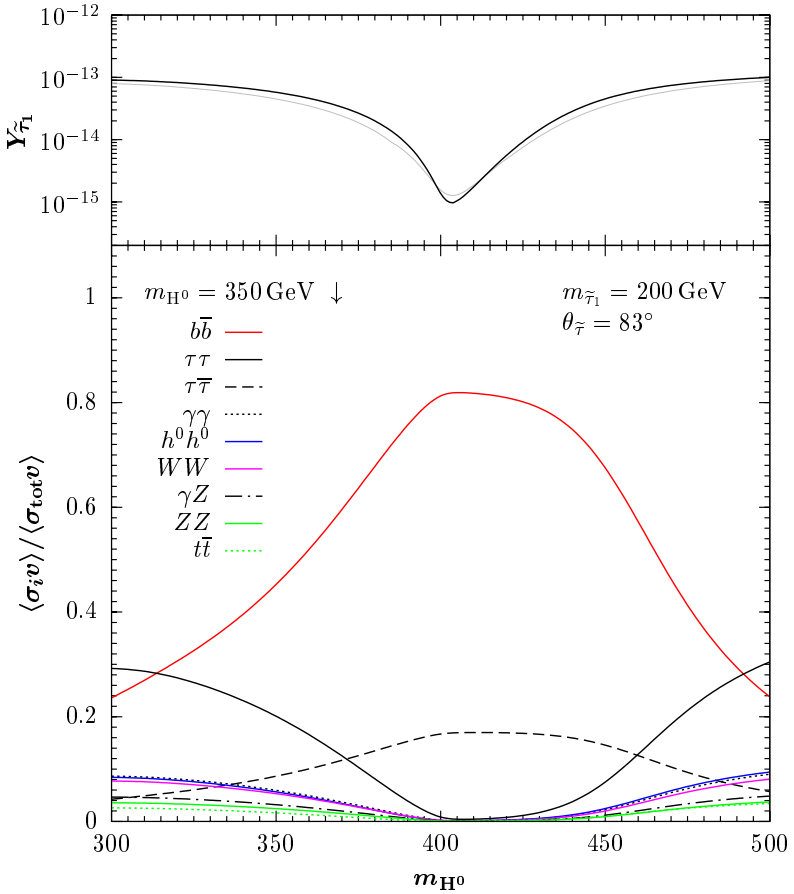

Figure 5: Dependence of $Y_{\widetilde{\tau}}$ (upper panel) and of $\langle\sigma_i v\rangle/\langle\sigma_{\rm tot} v\rangle$ at $x = 25$ (lower panel) on m_{H^0} for the pMSSM scenario associated with $m_{\widetilde{\tau}_1} = 200$ GeV, $\theta_{\widetilde{\tau}} = 83°$, $\tan\beta = 40$, and $-A = \mu = 4M_1 = M_{2,3} = M_S = 1$ TeV. In the upper panel, the dark line shows the stau yield $Y_{\widetilde{\tau}}$ obtained with our relic abundance calculation and the thin gray line the one obtained with `micrOMEGAs`. The stau decoupling yield takes on its minimum value of $Y_{\widetilde{\tau}} = 9.7 \times 10^{-16}$ at $m_{H^0} = 404$ GeV. In the lower panel, the displayed dominant stau annihilation channels are associated with the following final states: $b\bar{b}$, $\tau\tau$, $\tau\overline{\tau}$, $\gamma\gamma$, h^0h^0, WW, γZ, ZZ, and $t\bar{t}$ (at $m_{H^0} = 350$ GeV, from top to bottom).

$\sim m_f s_{\beta-\alpha} \tan\beta$ with $f = b, \tau$ [71]. The (broad) peak associated with the resonance[13] already builds up for $m_{H^0} > 2m_{\widetilde{\tau}_1} = 400$ GeV. At zero relative velocity, this would be a region in which the H^0 resonance cannot occur. However, since $\widetilde{\tau}_1$ is in kinetic equilibrium at the time of freeze out, resonant annihilation takes place already for $2m_{\widetilde{\tau}_1} < m_{H^0}$ [79]. For $m_{H^0} < 2m_{\widetilde{\tau}_1} = 400$ GeV, the processes containing s-channel H^0 exchange proceed with a slightly faster rate (if kinematically allowed). The impact of the H^0 resonance on the thermal $\widetilde{\tau}_1$ freeze out and the resulting $Y_{\widetilde{\tau}}$ is substantial. Since the total width of H^0 is $\Gamma_{H^0} = (6 - 10)$ GeV for $m_{H^0} = (300 - 500)$ GeV in the considered pMSSM scenario, the reduction of $Y_{\widetilde{\tau}}$ extends over a relatively large m_{H^0} range. In this regard, note that Γ_{H^0} could be substantially larger had we not essentially decoupled all sfermions—except

[13] Notice that we plot $\langle\sigma_i v\rangle/\langle\sigma_{\rm tot} v\rangle$ so that the actual shape of the resonance looks somewhat different.

$\widetilde{\tau}_1$, $\widetilde{\tau}_2$, and $\widetilde{\nu}_\tau$—by choosing $M_S = 1$ TeV. For $m_{H^0} \simeq 404$ GeV, i.e., at the dip of the resonance, we find $x_\mathrm{f} \simeq 33$ and a minimum stau decoupling yield of $Y_{\widetilde{\tau}} = 9.7 \times 10^{-16}$ (dark line). Thus, despite the (still) moderate value of $\tan\beta = 40$, a significant reduction of $Y_{\widetilde{\tau}}$ is encountered. Indeed, $Y_{\widetilde{\tau}}$ can be even further suppressed for a larger value of $\tan\beta$. Let us remark that an accurate determination of $Y_{\widetilde{\tau}}$ in the resonance region requires to take special care of the $b\overline{b}H^0$ vertex. This coupling is well known to receive substantial radiative corrections for sizable values of $\tan\beta$. Therefore, we rely again on the computer tool `FeynHiggs` to compute all quark–antiquark–Higgs couplings and the total width Γ_{H^0}. Also the `micrOMEGAs` code takes special care of the $b\overline{b}H^0$ vertex. We therefore think that the difference between the yields shown in the upper panel of Fig. 5 reflects the theoretical uncertainty involved in the determination of Γ_{H^0} as well as the $b\overline{b}H^0$ vertex.

7. On the viability of a $\widetilde{\tau}_1$-$\widetilde{\tau}_1^*$ asymmetry

Given the strong bounds on the abundance of negatively charged $\widetilde{\tau}_1$ from bound-state effects during BBN, i.e., from CBBN of ^{6}Li and ^{9}Be, it is natural to ask whether it is possible to have an excess of positively charged $\widetilde{\tau}_1^*$'s over negatively charged $\widetilde{\tau}_1$'s. The generation of a particle-antiparticle asymmetry requires a departure from thermal equilibrium. Therefore, one might think that a $\widetilde{\tau}_1$-$\widetilde{\tau}_1^*$ asymmetry can be produced at the time of the stau freeze out if the (slepton number violating) process $\widetilde{\tau}_1\widetilde{\tau}_1 \to \tau\tau$ occurs at a different rate than its conjugate counterpart. Such a situation might indeed occur if we allow for (CP-violating) complex values of the parameters A_τ, μ, and $M_{1,2}$ in the SUSY sector. However, the staus are still tightly coupled to Standard Model particles so that they remain in kinetic equilibrium with the primordial plasma. Therefore, any excess of $\widetilde{\tau}_1^*$ over $\widetilde{\tau}_1$ arising will be washed out quickly by the inelastic scattering process $\widetilde{\tau}_1^*\tau \leftrightarrow \widetilde{\tau}_1\overline{\tau}$.[14] Indeed, it is well-known [79] that processes of the latter type occur at much larger rates than the rates for the mutual annihilation of the decoupling particle species. The same argument given in [79] can be adopted to our case. At the time of freeze out, the reaction rates of interest can be estimated as

$$\widetilde{\tau}_1\widetilde{\tau}_1 \to \tau\tau : \quad n_{\widetilde{\tau}_1} n_{\widetilde{\tau}_1} \sigma_{\widetilde{\tau}_1\widetilde{\tau}_1\to\tau\tau} \sim T^3 m_{\widetilde{\tau}_1}^3 e^{-2m_{\widetilde{\tau}_1}/T} \sigma_{\widetilde{\tau}_1\widetilde{\tau}_1\to\tau\tau} \,, \tag{7.1}$$

$$\widetilde{\tau}_1^*\tau \to \widetilde{\tau}_1\overline{\tau} : \quad n_{\widetilde{\tau}_1^*} n_\tau \sigma_{\widetilde{\tau}_1^*\tau\to\widetilde{\tau}_1\overline{\tau}} \sim T^{9/2} m_{\widetilde{\tau}_1}^{3/2} e^{-m_{\widetilde{\tau}_1}/T} \sigma_{\widetilde{\tau}_1^*\tau\to\widetilde{\tau}_1\overline{\tau}} \,, \tag{7.2}$$

since $\widetilde{\tau}_1^{(*)}$ is approximately Boltzmann distributed. For simplicity, we have treated the tau lepton τ as a (still) relativistic species. By taking the ratio of (7.2) with respect to (7.1),

$$(T/m_{\widetilde{\tau}_1})^{3/2}\, e^{m_{\widetilde{\tau}_1}/T} \sim 10^9 \quad \text{for} \quad m_{\widetilde{\tau}_1}/T \simeq 25 \,, \tag{7.3}$$

we find that the equilibrating process is by far more dominant. Here, we have used that $\sigma_{\widetilde{\tau}_1\widetilde{\tau}_1\to\tau\tau}$ and $\sigma_{\widetilde{\tau}_1^*\tau\to\widetilde{\tau}_1\overline{\tau}}$ are not too different. In fact, both processes proceed at tree level exclusively via $\widetilde{\chi}_i^0$ exchange so that one cannot decouple (7.2) from (7.1) by a simple adjustment of the neutralino mass spectrum.

[14] We are grateful to M. Pospelov for pointing out that process. Additional equilibrating processes are, e.g., $\widetilde{\tau}_1^* W^- \leftrightarrow \widetilde{\tau}_1 W^+$ or $\widetilde{\tau}_1^* H^- \leftrightarrow \widetilde{\tau}_1 H^+$, which are however Boltzmann-suppressed. Also note that a lepton asymmetry of the order of the baryon asymmetry is expected in baryogenesis scenarios based on leptogenesis.

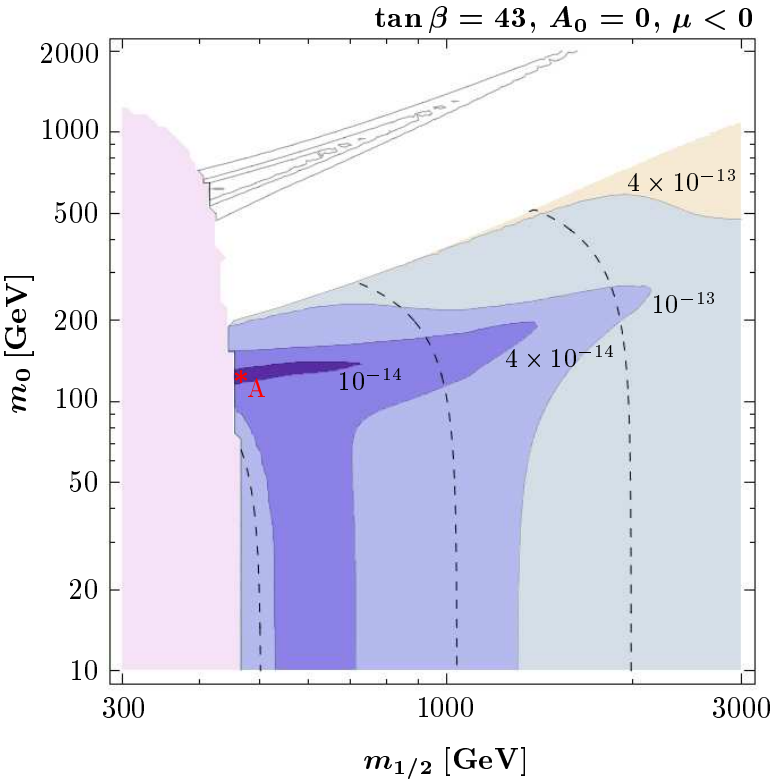

Figure 6: Contours of $Y_{\widetilde{\tau}}$ (as labeled) in the $(m_{1/2}, m_0)$ plane for $\tan\beta = 43$, $A_0 = 0$, and $\mu < 0$, where darker shadings imply smaller $Y_{\widetilde{\tau}}$ values. The dashed lines are contours of $m_{\widetilde{\tau}_1} = 100$, 300, and 600 GeV (from left to right). The light-shaded region at $m_{1/2} \lesssim 450$ GeV is excluded by the LEP bound $m_{h^0} \leq 114.4$ GeV [1]. In the white area either $m_{\widetilde{\chi}_1^0} < m_{\widetilde{\tau}_1}$ or correct electroweak symmetry breaking is not established (in the very upper left corner), where the thin contours indicate the Higgs funnel in the $\widetilde{\chi}_1^0$ LOSP region. Table 2 provides detailed information for the SUSY model represented by the point "A" that is indicated by the star.

8. Exceptionally small stau abundances within the CMSSM

We have shown above that the total stau annihilation cross section can be significantly enhanced. The thermal freeze out of $\widetilde{\tau}_1$'s is thereby delayed such that their abundance prior to decay, $Y_{\widetilde{\tau}}$, is suppressed. In the following we focus on the CMSSM to see whether the effects discussed in Sects. 5 and 6 do appear also in models in which the pattern of soft-SUSY breaking parameters fulfills certain boundary conditions at a high scale. Note that we compute $Y_{\widetilde{\tau}}$ with `micrOMEGAs` in this section since coannihilation processes are not included in our relic density code. In addition, we employ `SPheno 2.2.3` [80] for the computation of the mass spectrum and the low energy constraints associated with $B(b \to s\gamma)$ and the anomalous magnetic moment of the muon a_μ. Let us now proceed by discussing two exemplary CMSSM parameter scans.

Figure 6 shows contours of constant $Y_{\widetilde{\tau}}$ in the $(m_{1/2}, m_0)$ plane for $\tan\beta = 43$, $A_0 = 0$, and a negative sign of the μ parameter. The contour lines represent the values $Y_{\widetilde{\tau}} = 10^{-14}$,

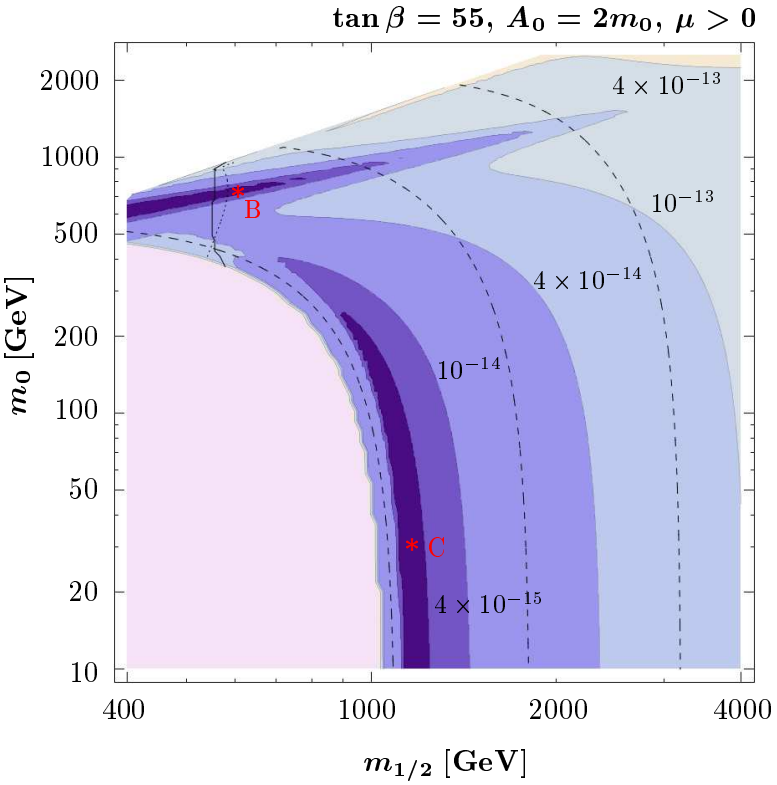

Figure 7: Contours of $Y_{\tilde{\tau}}$ (as labeled) in the $(m_{1/2}, m_0)$ plane for $\tan\beta = 55$, $A_0 = 2m_0$, and $\mu > 0$, where darker shadings imply smaller $Y_{\tilde{\tau}}$ values. The dashed lines are contours of $m_{\tilde{\tau}_1} =$ 100, 300, and 600 GeV (from left to right). The large light-shaded region in the lower left corner is excluded by bounds from direct Higgs and SUSY searches (or by the appearance of a tachyonic spectrum). In the region to the left of the vertical solid and dotted lines, $m_{h^0} \leq 114.4$ GeV [1] and $B(b \to s\gamma) \geq 4.84 \times 10^{-4}$ [81], respectively. In the white area, $m_{\tilde{\chi}_1^0} < m_{\tilde{\tau}_1}$. Table 2 provides detailed information for the SUSY models represented by the stars "B" and "C" (as labeled).

4×10^{-14}, 10^{-13}, and 4×10^{-13}, where darker shadings imply smaller values of $Y_{\tilde{\tau}}$. The dashed lines are contours of $m_{\tilde{\tau}_1} = 100$, 300 and 600 GeV (from left to right). The light-shaded region at $m_{1/2} \lesssim 450$ GeV is excluded by the mass bound $m_{h^0} \geq 114.4$ GeV from Higgs searches at LEP [1]. The white area indicates the region in which either correct electroweak symmetry breaking is not established (in the very upper left corner) or in which $m_{\tilde{\chi}_1^0} < m_{\tilde{\tau}_1}$. Since $\mu < 0$, the plane is actually in tension because of (negative) SUSY contributions $a_\mu^{\rm SUSY}$ to the anomalous magnetic moment of the muon, $a_\mu \equiv (g-2)_\mu/2$.

Figure 7 presents a scan over the $(m_{1/2}, m_0)$ plane for $\tan\beta = 55$, $A_0 = 2m_0$, and $\mu > 0$ with contours of $Y_{\tilde{\tau}} = 4 \times 10^{-15}$, 10^{-14}, 4×10^{-14}, 10^{-13}, and 4×10^{-13} (darker shadings indicate smaller $Y_{\tilde{\tau}}$ values) and $m_{\tilde{\tau}_1} = 100$, 300, and 600 GeV (dashed lines, from left to right). The large light-shaded region in the lower left corner is excluded by the robust bound $m_{\tilde{\tau}_1} \geq 82$ GeV [1] from collider searches of charged sleptons (or by the appearance of a tachyonic spectrum). The LEP Higgs bound $m_{h^0} \leq 114.4$ GeV [1] is situated within this region in close vicinity to its boundary for $m_0 \lesssim 400$ GeV and is indicated by the solid line

for $m_0 \gtrsim 400$ GeV. In the region to the left of the dotted line, $B(b \to s\gamma) \geq 4.84 \times 10^{-4}$ [81], which is in tension with the bounds from inclusive $b \to s\gamma$ decays.

Let us now discuss some generic features of the stau yield within the CMSSM on the basis of Figs. 6 and 7. We note beforehand that our more general statements on the $\widetilde{\tau}_1$ LOSP region in the CMSSM are corroborated by a parameter scan over the following range[15]

$$\begin{aligned} m_{1/2} &= (0.1 - 6)\ \text{TeV}, \qquad & \tan\beta &= 2 - 60, \\ -4m_0 &< A_0 < 4m_0, & \operatorname{sgn}\mu &= \pm 1. \end{aligned} \tag{8.1}$$

In both figures an almost horizontal, narrow band of low $Y_{\widetilde{\tau}}$ appears in which $2m_{\widetilde{\tau}_1} \simeq m_{H^0}$ holds so that stau annihilation proceeds via resonant production of the heavy CP-even Higgs boson H^0. We have marked points the centers of the respective regions with "A" and "B" for which we provide detailed information in Table 2. Given a present uncertainty of ~ 3 GeV in the determination of m_{h^0} [82], we note that the LEP Higgs bound has to be treated with some care. For example, a (vertical) $m_{h^0} = 112$ GeV contour would be situated at $m_{1/2} \simeq 400$ GeV in the resonance region of Fig. 7. Accordingly, one could consider the entire resonance region shown to be compatible with direct Higgs searches. However, due to the large value of $\tan\beta = 55$, the bound on $b \to s\gamma$ is very strong so that a large part of the resonance region remains excluded by this constraint. In this regard, it is interesting to see (Fig. 6) that $2m_{\widetilde{\tau}_1} \simeq m_{H^0}$ also appears in the $\widetilde{\tau}_1$ LOSP region for lower values of $\tan\beta$. In the center of both resonance regions, the yield becomes as low as $Y_{\widetilde{\tau}} = 4.2 \times 10^{-15}$ (point A) and $Y_{\widetilde{\tau}} = 2.5 \times 10^{-15}$ (point B). Despite the heavier mass of the lighter stau (see Table 2), the suppression of $Y_{\widetilde{\tau}}$ is still more pronounced in Fig. 7 than in Fig. 6. This is because the bottom Yukawa coupling becomes larger with increasing $\tan\beta$, as discussed already in Sect. 6. In fact, annihilation into $b\overline{b}$ final states is in both cases by far the dominant process with relative importances of 76% (point A) and 87% (point B). The extension of both resonance regions is due to the total width of H^0 of respectively $\Gamma_{H^0} \simeq 9.6$ GeV (point A) and $\Gamma_{H^0} \simeq 22$ GeV (point B); note the logarithmic scales in Figs 6 and 7. We note in passing that the appearance of the H^0 resonance does not imply the absence of the neutralino funnel region which is indicated by the (unshaded) contour lines in the white area of Fig. 6

Of course, the question arises whether the appearance of the resonance region is encountered more generically within the framework of the CMSSM. In principle, it is not easy to provide a simple quantitative connection between $m_{\widetilde{\tau}_1}$ and m_{H^0} for arbitrary values of the CMSSM parameters. However, without emphasis on an overall applicability, a qualitative picture can be drawn. Let us start with the mass of the CP-odd Higgs boson m_{A^0} which can be written as [83, 84]

$$m_{A^0}^2 \sim 1/\sin^2\beta\,(m_0^2 + 0.52 m_{1/2}^2 + \mu^2 - \dots). \tag{8.2}$$

Here, the ellipsis stand for contributions from the bottom and tau Yukawa couplings. For $\tan\beta \gtrsim 20$, $m_{A^0}^2 \sim m_0^2 + 2.5 m_{1/2}^2 - \dots$, and the corrections from the bottom and tau

[15] Here, we disregard CMSSM parameter points in which `SPheno` flags an error in the spectrum calculation.

Yukawa couplings become important so that m_{A^0} is driven towards lower values;[16] note that $\sin^2\beta \simeq 1$ for $\tan\beta \gtrsim 20$. Indeed, this property can be used to constrain $\tan\beta$ from above by confronting m_{A^0} with the lower bound from LEP, $m_{A^0} > 93.4$ GeV [1]. On the other hand, for large $m_{1/2}$, one also enters the decoupling limit of the MSSM so that m_{A^0} and m_{H^0} will be nearly degenerate in mass; cf. (4.1). This can be also seen from the exemplary points presented in Table 2. Therefore, also m_{H^0} will be driven towards lower values for growing $\tan\beta$. Now, left-right mixing of the lighter stau for not too large values of $\tan\beta$ is small within the CMSSM, $\widetilde{\tau}_1 \simeq \widetilde{\tau}_\mathrm{R}$, so that approximately $m^2_{\widetilde{\tau}_1} \sim m_0^2 + 0.15 m^2_{1/2}$ [84]. Therefore, $2m_{\widetilde{\tau}_1} < m_{H^0}$ is the relation that holds usually in the region in which $\widetilde{\tau}_1$ is the lightest Standard Model superpartner. However, for large $\tan\beta$, the contributions from the bottom Yukawa coupling in (8.2) can become strong enough (growing with m_0 [84]) to overcome any additional decrease of $m_{\widetilde{\tau}_1}$ due to left-right mixing so that the resonance condition $2m_{\widetilde{\tau}_1} \simeq m_{H^0}$ can indeed be met. Nevertheless, from scanning over the CMSSM parameter range (8.1) it seems to us that the resonance condition $2m_{\widetilde{\tau}_1} \simeq m_{H^0}$ is not easily realized in the part of the $\widetilde{\tau}_1$ LOSP region in which $\widetilde{\tau}_1$-$\widetilde{\chi}^0_1$ coannihilations are negligible. Conversely, it is clear that relaxing the universality conditions for the soft-SUSY breaking masses at M_GUT will make it easier to find parameter regions in which the resonance condition $2m_{\widetilde{\tau}_1} \simeq m_{H^0}$ is satisfied. Of particular interest in this respect is the model with non-universal Higgs masses (NUHM) with $m_{H_1} \neq m_{H_2} \neq m_0$ at M_GUT. There, one can adjust the input parameters in order to realize resonant stau annihilation. Indeed, this model is qualitatively the same as the class of pMSSM scenarios considered in the previous sections, where m_{H_1} and m_{H_2} are traded (at the low-scale) against m_{A^0} and μ by using the electroweak symmetry breaking conditions.

Low $Y_{\widetilde{\tau}}$ values are also realized in the narrow vertical region around $m_{1/2} \sim 1.1$ TeV in Fig. 7. At the representative point "C" of that region, $Y_{\widetilde{\tau}} = 2.2 \times 10^{-15}$ and the main stau annihilation channels are the ones into h^0h^0 (90%) and WW (6%); see Table 2. For larger values of $m_{1/2}$, $Y_{\widetilde{\tau}}$ exhibits its well known behavior and grows with $m_{\widetilde{\tau}_1}$. To the left of the $Y_{\widetilde{\tau}} = 4\times10^{-15}$ contour, the yield increases quickly since the annihilation into h^0h^0 becomes kinematically forbidden. Indeed, regions of low $Y_{\widetilde{\tau}}$ which are due to the aforementioned annihilation channels are a commonplace appearance in the CMSSM parameter space. They are found slightly above the lowest feasible values of $m_{1/2}$, i.e., close to the boundary of the region which is excluded by direct Higgs and SUSY searches and where $m_{\widetilde{\tau}_1} > m_{h^0}$ still holds. This is because $\widetilde{\tau}_1$ is light in that region since the SUSY particle spectrum scales with $m_{1/2}$ (typically, $m_0 \ll m_{1/2}$ for $\widetilde{\tau}_1$ LOSP). Moreover, we find that the LEP Higgs bound drops hardly below $m_{1/2} \simeq 450$ GeV for $\tan\beta \gtrsim 40$ and $m_0 \lesssim 100$ GeV.[17] Due to a strong correlation between the gaugino mass parameter $m_{1/2}$ and the size of the μ parameter, $\mu^2 \sim (1-3)\, m^2_{1/2}$ [85], the value of μ in the experimentally allowed region is large. Recall from Sect. 5 that the $\widetilde{\tau}_1\widetilde{\tau}_1h^0$ coupling is $\sim \sin 2\theta_{\widetilde{\tau}} X_\tau$ ($m_{A^0} \gg M_\mathrm{Z}$) so that $|X_\tau| = |A_\tau - \mu\tan\beta|$ will become sizeable by increasing $\tan\beta$. This leads then

[16] The latter relation ignores contributions from A-terms which can be important but complicate the envisaged illustrative picture; for the derivation, we have used $m_\mathrm{t}(m_\mathrm{t}) = 163$ GeV in Eq. (2.25a) of Ref. [84].

[17] The position of the LEP Higgs bound (which appears as a near to vertical line for low m_0) is very sensitive to the value of m_t. Lowering m_t shifts the bound towards larger values of $m_{1/2}$.

to efficient stau annihilation into h^0h^0 final states. Indeed, in those CMSSM regions, also $|\sin 2\theta_{\widetilde{\tau}}|$ is maximized so that $Y_{\widetilde{\tau}}$ already starts to drop below the estimate (1.1) for $\tan\beta \gtrsim 40$. Note, however, that the left-right mixing of $\widetilde{\tau}_1$ within the CMSSM is somewhat constrained. Neglecting τ-Yukawa contributions, the RG-evolution induced splitting reads $m^2_{\widetilde{\tau}_L} - m^2_{\widetilde{\tau}_R} \sim 0.37 m^2_{1/2}$ [84] and indeed $\widetilde{\tau}_1$ remains mainly right-handed: By scanning over the parameter space, we typically find $65^\circ \lesssim \theta_{\widetilde{\tau}} \lesssim 115^\circ$ and thus $|\sin 2\theta_{\widetilde{\tau}}| \lesssim 0.75$ in the $\widetilde{\tau}_1$ LOSP region in which $m_{\widetilde{\tau}_1} > m_{h^0}$ and $m_{h^0} > 114.4$ GeV holds.

9. Prospects for collider phenomenology

If a SUSY model with a long-lived $\widetilde{\tau}_1$ of $m_{\widetilde{\tau}_1} < 0.7$ TeV is realized in nature, the $\widetilde{\tau}_1$ discovery potential will be promising at the LHC with a luminosity of 100 fb^{-1} [86]. For $m_{\widetilde{\tau}_1} < 0.25$ TeV (0.5 TeV), $\widetilde{\tau}_1$'s can also be examined in precision studies at the ILC with a c.m. range up to $\sqrt{s} = 0.5$ TeV (1 TeV). Once long-lived $\widetilde{\tau}_1$'s are produced, one should be able to distinguish them from muons by considering the associated highly ionizing tracks and with time-of-flight measurements. One should then also be able to infer $m_{\widetilde{\tau}_1}$ from measurements of the $\widetilde{\tau}_1$ velocity and its momentum [15] and complementary from (threshold) studies of the process $e^+e^- \to \widetilde{\tau}_1\widetilde{\tau}_1^*$ at the ILC.

Remarkably, both mechanisms leading to exceptionally small $Y_{\widetilde{\tau}}$ values come with testable predictions: certain ranges of the stau-mixing angle $\theta_{\widetilde{\tau}}$ together with large values of $\tan\beta$, $|\mu|$, and/or $|A_\tau|$ and, in the case of resonant stau annihilation, also $m_{H^0} \simeq 2m_{\widetilde{\tau}_1}$. In particular, the large stau-Higgs couplings lead to an enhanced production of light Higgs bosons in association with staus via $e^+e^- \to \widetilde{\tau}_1\widetilde{\tau}_1^* h^0$ and $\gamma\gamma \to \widetilde{\tau}_1\widetilde{\tau}_1^* h^0$. The associated cross sections can then be relatively large at the ILC with a sufficiently high c.m. energy [87]. In addition, the above reactions with H^0 instead of h^0 in the final state can have also relatively large cross sections if H^0 and $\widetilde{\tau}_1$ are sufficiently light. These reactions will then allow for an experimental determination of the stau-Higgs couplings and clarify whether its values are compatible with an extremely small value of $Y_{\widetilde{\tau}}$ [87]. Moreover, a measurement of m_{H^0} pointing to $m_{H^0} \simeq 2m_{\widetilde{\tau}_1}$ could be an experimental hint for resonant stau annihilation in the early Universe.

Indeed, the scenarios considered could allow for a determination of both m_{h^0} and m_{H^0} already at the LHC. Because of the large values of $\tan\beta$, the dominant production mechanism for h^0/H^0 will be the associated production of the neutral Higgs bosons with bottom quark pairs, $pp \to b\bar{b}h^0/H^0$; see, e.g., [88, 89, 90, 91] and references therein. In fact, associated $b\bar{b}h^0/H^0$ production with $h^0/H^0 \to \mu^+\mu^-$ is considered as one of the most promising processes for measurements of m_{H^0} at the LHC despite the relatively small $h^0/H^0 \to \mu^+\mu^-$ branching ratio [92]. In SUSY scenarios with a sufficiently light long-lived $\widetilde{\tau}_1$ LOSP, these processes will be complemented by associated $b\bar{b}h^0/H^0$ production with $h^0/H^0 \to \widetilde{\tau}_1\widetilde{\tau}_1^*$, where measurements of the invariant mass of the $\widetilde{\tau}_1\widetilde{\tau}_1^*$ pair could potentially provide a unique way to infer m_{h^0} and m_{H^0} at the LHC. In fact, $h^0/H^0 \to \widetilde{\tau}_1\widetilde{\tau}_1^*$ will occur most prominently exactly in the regions associated with the exceptional $Y_{\widetilde{\tau}}$ values due to the enhanced stau–Higgs couplings. Having outlined these proposals, we leave a dedicated study for future work.

Table 2 illustrates that the kinematical reach of both the LHC and the ILC could be sufficiently large to allow for the studies mentioned above. In none of the given points does $m_{\widetilde{\tau}_1}$ exceed 200 GeV so that $\widetilde{\tau}_1\widetilde{\tau}_1^*$ pair production would already be possible at the ILC with $\sqrt{s} \leq 0.5$ TeV. There, one could also produce $\widetilde{\tau}_1\widetilde{\tau}_1^* h^0$ final states in scenarios A and C. Even the condition $m_{H^0} \simeq 2m_{\widetilde{\tau}_1}$ could be probed in both scenarios A and B that allow for resonant stau annihilation.

10. Implications for gravitino dark matter scenarios

As already stressed in the Introduction, $Y_{\widetilde{\tau}}$ is subject to stringent cosmological constraints. Indeed, to decide on the cosmological viability of a SUSY model, one has to confront the associated $Y_{\widetilde{\tau}}$ values with those constraints. In particular, for gravitino LSP scenarios with unbroken R-parity, restrictive cosmological constraints and implications thereof have been derived [48, 39, 40, 41, 57, 42, 32, 93, 36] often under the assumption that $Y_{\widetilde{\tau}}$ can be described by (1.1). However, while (1.1) is quite reliable for $\widetilde{\tau}_1 \simeq \widetilde{\tau}_{\rm R}$ [37, 38, 40, 52], we have shown in the previous sections that $Y_{\widetilde{\tau}}$ (for a given $m_{\widetilde{\tau}_1}$) can be about than two orders of magnitude smaller than (1.1). Thus, in gravitino dark matter scenarios with such exceptionally small $Y_{\widetilde{\tau}}$ values, our understanding of the cosmological constraints and the associated implications could change significantly.

To demonstrate this point, let us indicate for which $Y_{\widetilde{\tau}}$ values the existing cosmological constraints (in their present status) are respected:

- For $Y_{\widetilde{\tau}} < 10^{-14}$, the upper limit on $Y_{\widetilde{\tau}}$ imposed by the non-thermal production of gravitinos in $\widetilde{\tau}_1$ decays, $\Omega_{\widetilde{G}}^{\rm NTP} \leq f\,\Omega_{\rm dm}$—given explicitly in (22) of Ref. [22]—is respected for $m_{\widetilde{G}} \lesssim 500$ GeV even if only a small fraction $f = 0.01$ of dark matter is assumed to originate from $\widetilde{\tau}_1$ decays; cf. Fig. 13 of Ref. [22]. This applies equally to other scenarios with an extremely weakly interacting LSP—such as the axino LSP [5, 19]—originating from $\widetilde{\tau}_1$ decays.

- For $Y_{\widetilde{\tau}} \lesssim 10^{-13}$, the BBN constraints associated with effects of hadronic energy release on the primordial D abundance can be respected for $\widetilde{\tau}_1 \simeq \widetilde{\tau}_{\rm R}$ and $m_{\widetilde{\tau}_1}$ up to 10 TeV independent of the $\widetilde{\tau}_1$ lifetime; cf. Fig. 11 of Ref. [22]. For a sizable admixture of $\widetilde{\tau}_{\rm L}$ in $\widetilde{\tau}_1$, this $Y_{\widetilde{\tau}}$ constraint can become more restrictive in particular with the enhanced stau–Higgs couplings allowing for exceptionally small $Y_{\widetilde{\tau}}$ values. Nevertheless, these exceptional values are typically associated with $m_{\widetilde{\tau}_1} < 300$ GeV where the $Y_{\widetilde{\tau}}$ limit is significantly more relaxed: $Y_{\widetilde{\tau}} \lesssim 10^{-11}$ for $\widetilde{\tau}_1 \simeq \widetilde{\tau}_{\rm R}$. A tightening to $Y_{\widetilde{\tau}} \lesssim 10^{-13}$ (10^{-15}) will then require an increase of $\epsilon_{\rm had}$ by a factor of 10^2 (10^4). On the other hand, sufficiently degenerate $m_{\widetilde{G}}$ and $m_{\widetilde{\tau}_1}$ will always be associated with small values of $\epsilon_{\rm had}$ and thereby with relaxed $Y_{\widetilde{\tau}}$ limits from energy release, even in the case of strongly enhanced stau–Higgs couplings.

- For $Y_{\widetilde{\tau}} \lesssim 10^{-14}$ (10^{-15}), the BBN constraints associated with effects of electromagnetic energy release on the primordial D (^{3}He) abundance can be respected independent of the $\widetilde{\tau}_1$ lifetime; cf. upper panels of Fig. 12 (100 GeV $\leq m_{\widetilde{\tau}_1} \leq$ 10 TeV) of Ref. [22] and Figs. 14 ($m_{\widetilde{\tau}_1} = 100$ GeV) and 15 ($m_{\widetilde{\tau}_1} = 300$ GeV) of Ref. [32].

- For $Y_{\widetilde{\tau}} \lesssim 2\times10^{-15}$ ($2\times10^{-16}-2\times10^{-15}$), the BBN constraints associated with bound state effects allowing for CBBN of ^{9}Be (^{6}Li) can be respected even for $\tau_{\widetilde{\tau}_1} \gtrsim 10^5\,\mathrm{s}$; cf. Fig. 5 in Ref. [36]. The uncertainty on the $Y_{\widetilde{\tau}}$ limit associated with CBBN of ^{6}Li reflects the difficulties in quantifying an upper limit on the primordial ^{6}Li abundance; for more details on this issue, see [36] and references therein. Note that the given limits correspond to upper limits on the primordial fractions of ^{9}Be/H and ^{6}Li/H of 2.1×10^{-13} and $10^{-11}-10^{-10}$, respectively.

Thus, the SUSY models which come with thermal relic stau abundances of $Y_{\widetilde{\tau}} \lesssim 2\times10^{-15}$ can respect each of these cosmological constraints independent of the stau lifetime if a primordial ^{6}Li/H abundance of about 10^{-10} is viable. In particular, the limit of $\tau_{\widetilde{\tau}_1} \lesssim 5\times10^3\,\mathrm{s}$ and its implications—discussed in the Introduction—are then no longer valid even for a standard cosmological history with primordial temperatures of $T > T_\mathrm{f}$. Thereby, the regions with $Y_{\widetilde{\tau}} \lesssim 2\times10^{-15}$ are associated with particularly attractive gravitino dark matter scenarios:

- The gravitino mass can be within the range $0.1 \lesssim m_{\widetilde{G}} < m_{\widetilde{\tau}_1}$ for which its kinematical determination could be viable [16, 21, 24]. Together with measurements of $m_{\widetilde{\tau}_1}$ and $\tau_{\widetilde{\tau}_1}$, a kinematically determined $m_{\widetilde{G}}$ would allow one to measure the Planck scale $\mathrm{M_P}$ at colliders [16, 21, 24]. Indeed, an agreement of the $\mathrm{M_P}$ value determined in collider experiments with the one inferred from Newton's constant G_N would support the existence of supergravity in nature [16].

- For $m_{\widetilde{G}}$ sufficiently close to $m_{\widetilde{\tau}_1}$, the spin 3/2 character of the gravitino becomes relevant so that it could be probed in principle by analyzing the decays $\widetilde{\tau}_1 \to \widetilde{G}\tau\gamma$ [16].

- With $Y_{\widetilde{\tau}} \lesssim 2\times10^{-15}$, $\Omega_{\widetilde{G}}^{\mathrm{NTP}}$ is negligible so that basically all of Ω_dm can be provided by gravitinos from other sources such as thermal production [25, 27, 28]. Indeed, if also gravitino production in decays of scalar fields such as the inflaton [94, 95] is negligible, reheating temperatures of $T_\mathrm{R} \lesssim 10^9\,\mathrm{GeV}$ could become viable for $m_{\widetilde{G}} \sim 100\,\mathrm{GeV}$ and not too heavy gaugino masses [40, 28]. This would mean that thermally produced gravitinos could provide the right amount of dark matter and that thermal leptogenesis [43] with hierarchical heavy Majorana neutrinos—which typically requires $T_\mathrm{R} \gtrsim 10^9\,\mathrm{GeV}$ [44, 45, 46, 47]—would be a viable explanation of the cosmic baryon asymmetry, i.e., there would be no gravitino problem.

- With a kinematically determined $m_{\widetilde{G}}$, one would be able to probe the reheating temperature T_R at colliders and thereby the viability of thermal leptogenesis [27].

- For $\tau_{\widetilde{\tau}_1} \gtrsim 10^4\,\mathrm{s}$, the small $Y_{\widetilde{\tau}}$ values could still allow for the primordial catalysis of ^{6}Li and ^{9}Be in agreement with existing astrophysical observations [33, 34, 35, 36].

Table 2 illustrates that gravitino dark matter scenarios of the type discussed above can even be accommodated within the CMSSM.[18] For gravitino masses of 50 GeV and

[18]Note that this finding points to a caveat of our earlier study [41] relying on $\tau_{\widetilde{\tau}_1} \lesssim 5\times10^3\,\mathrm{s}$ derived from the assumption that $Y_{\widetilde{\tau}}$ is described by (1.1). Our previous sections however show that islands exist in which $Y_{\widetilde{\tau}}$ can be significantly below (1.1) even within the CMSSM and for a standard cosmological history.

100 GeV, we list the associated values of $\tau_{\widetilde{\tau}_1}$, of $\Omega_{\widetilde{G}}^{\rm NTP}h^2$, and of the maximum reheating temperature $T_{\rm R}^{\rm max}$ under the assumption that other gravitino sources can be neglected. The expression for $\tau_{\widetilde{\tau}_1}$ can be found, e.g., in (8) of Ref. [41] whereas (12) of the same reference can be used to infer the $T_{\rm R}^{\rm max}$ values imposed by $\Omega_{\widetilde{G}}^{\rm TP}h^2 \leq 0.126$. At each CMSSM point and for both $m_{\widetilde{G}}$ values, $\widetilde{\tau}_1$ is very long lived, $\tau_{\widetilde{\tau}_1} > 10^6\,{\rm s}$, and gravitino production from $\widetilde{\tau}_1$ decays is negligible, $\Omega_{\widetilde{G}}^{\rm NTP}h^2 \lesssim 10^{-4}$. In all cases, the gravitino mass $m_{\widetilde{G}} = 100$ GeV is sufficiently close to $m_{\widetilde{\tau}_1}$ so that the spin 3/2 character of the gravitino can in principle be probed [16]. A reheating temperature of $T_{\rm R} \gtrsim 10^9\,{\rm GeV}$ is viable only for the points A and B with $m_{1/2}$ significantly below 1 TeV, i.e., at the points at which resonant stau annihilation leads to the reduction of $Y_{\widetilde{\tau}}$. Because of $\tau_{\widetilde{\tau}_1} > 10^6\,{\rm s}$, the $Y_{\widetilde{\tau}}$ limit from CBBN of ^{9}Be is at $Y_{\rm Be}^{\rm max} \simeq 2\times10^{-15}$ for each point as can be inferred from Fig. 5 of Ref. [36]. This bound disfavors point A while the points B and C are associated with $Y_{\widetilde{\tau}}$ values very close to this limit and thereby with ^{9}Be/H (^{6}Li/H) values of about 2.1×10^{-13} (10^{-10}) [36].

11. Conclusions

Supersymmetric models with a long-lived stau $\widetilde{\tau}_1$ being the lightest Standard Model superpartner are well-motivated and very attractive in light of potentially striking signatures at colliders. For a standard thermal history with primordial temperatures $T > m_{\widetilde{\tau}_1}/20 > T_{\rm f}$—which is the working hypothesis is this work—the long-lived $\widetilde{\tau}_1$ becomes an electrically charged thermal relic whose abundance can be restricted by cosmological constraints.

We have carried out a thorough study of primordial stau annihilation and the associated thermal freeze out. Taking into account the complete set of stau annihilation channels within the MSSM with real parameters for cases with negligible sparticle coannihilation, the resulting thermal relic $\widetilde{\tau}_1$ yield $Y_{\widetilde{\tau}}$ has been examined systematically. While related earlier studies focussed mainly on the $\widetilde{\tau}_1 \simeq \widetilde{\tau}_{\rm R}$ case [37, 38, 40, 52], we have investigated cases in which $\widetilde{\tau}_1$ contains a significant admixture of $\widetilde{\tau}_{\rm L}$ including the maximal mixing case and $\widetilde{\tau}_1 \simeq \widetilde{\tau}_{\rm L}$.

We find that the variation of the stau mixing angle $\theta_{\widetilde{\tau}}$ does affect the relative importance of the different annihilation channels significantly but not necessarily the resulting $Y_{\widetilde{\tau}}$ value for relatively small values of $\tan\beta$. By increasing $\tan\beta$, however, we encounter a dramatic change of this picture for large absolute values of the Higgs-higgsino mass parameter μ and/or of the trilinear coupling A_τ, which are the dimensionful SUSY parameters that govern simultaneously stau left-right mixing and the stau–Higgs couplings: Stau annihilation into h^0h^0, h^0H^0, and H^0H^0 can become very efficient (if kinematically allowed) so that $Y_{\widetilde{\tau}}$ can decrease to values well below 10^{-15}. The scalar nature of $\widetilde{\tau}_1$ allows those parameters to enter directly into the annihilation cross sections. This mechanism has no analogue in calculations of the thermal relic density of the lightest neutralino $\widetilde{\chi}_1^0$.

The stau–Higgs couplings are crucial also for the second $Y_{\widetilde{\tau}}$ reduction mechanism identified in this work: Even for moderate values of $\tan\beta$, we find that staus can annihilate very efficiently into a $b\bar{b}$ pair via s-channel exchange of the heavy CP-even Higgs boson H^0 provided the MSSM spectrum exhibits the resonance condition $2m_{\widetilde{\tau}_1} \simeq m_{H^0}$. We have shown explicitly that the associated $Y_{\widetilde{\tau}}$ values can be below 10^{-15} as well. This mechanism

is similar to the one that leads to the reduction of the $\widetilde{\chi}_1^0$ density in the Higgs funnel region in which neutralino annihilation proceeds at the resonance of the CP-odd Higgs boson A^0.

We have worked with an effective low energy version of the MSSM to investigate the $\theta_{\widetilde{\tau}}$-dependence of $Y_{\widetilde{\tau}}$ and the two $Y_{\widetilde{\tau}}$-reduction mechanisms in a controlled way. In addition, we have shown that the considered effects can be accommodated also with restrictive assumptions on the soft-SUSY breaking sector at a high scale. Within the CMSSM, we encounter both mechanisms each of which leading to $Y_{\widetilde{\tau}} \simeq 2 \times 10^{-15}$ in two distinct regions of a single ($m_{1/2}$, m_0) plane.

We have discussed possibilities to probe the viability of the presented $Y_{\widetilde{\tau}}$-reduction mechanisms at colliders. While a m_{H^0} measurement pointing to $m_{H^0} \simeq 2m_{\widetilde{\tau}_1}$ would support resonant primordial stau annihilation, studies of Higgs boson production in association with staus, $e^+e^- (\gamma\gamma) \to \widetilde{\tau}_1\widetilde{\tau}_1^* h^0, \widetilde{\tau}_1\widetilde{\tau}_1^* H^0$ could allow for an experimental determination of the relevant stau–Higgs couplings, for example, at the ILC. Moreover, we have outlined that associated $b\bar{b}h^0/H^0$ production with $h^0/H^0 \to \widetilde{\tau}_1\widetilde{\tau}_1^*$ has the potential to allow for a determination of both m_{h^0} and m_{H^0} at the LHC if a SUSY scenario with large $\tan\beta$ and large stau–Higgs couplings is realized.

With the obtained small $Y_{\widetilde{\tau}}$ values, even the restrictive constraints associated with CBBN could be respected so that attractive gravitino dark matter scenarios could be revived to be cosmologically viable even for a standard cosmological history. Within this class of models, collider evidence for supergravity, for the gravitino being the LSP, and for high values of the reheating temperatures of up to 10^9 GeV is conceivable, which could thereby accommodate simultaneously the explanation of the cosmic baryon asymmetry provided by thermal leptogenesis and the hypothesis of thermally produced gravitinos being the dark matter in our Universe.

Acknowledgments – We are grateful to T. Hahn, J.-L. Kneur, and A. Pukhov for patient correspondence on their computer codes. Furthermore, we are grateful to T. Plehn, M. Pospelov, and Y.Y.Y. Wong for valuable discussions. This research was supported in part by the DFG cluster of excellence "Origin and Structure of the Universe."

Note added – Ref. [96], in which the potential suppression in the stau yield $Y_{\widetilde{\tau}}$ due to an enhanced annihilation into h^0h^0 final states is also studied, appeared as this work was being finalized. This paper provides analytic approximations for the stau annihilation cross section into h^0h^0 and for the associated yield. In addition, results of numerical studies within the CMSSM, the NUHM, and a scenario with non-universal gaugino masses are presented that exhibit parameter regions with extremely small $Y_{\widetilde{\tau}}$ values. In our work also enhanced stau annihilation into h^0H^0 and into H^0H^0 and stau annihilation at the H^0 resonance, which were not considered in [96], are discussed. In addition, our work provides a systematic investigation based on a complete set of stau annihilation channels, an outline of the way in which the mechanisms leading to the suppression of $Y_{\widetilde{\tau}}$ can be probed at collider experiments, and a thorough presentation of the potential implications for gravitino dark matter scenarios.

References

[1] **Particle Data Group** Collaboration, W. M. Yao *et. al.*, *Review of particle physics*, *J. Phys.* **G33** (2006) 1–1232.

[2] H. Pagels and J. R. Primack, *Supersymmetry, cosmology and new tev physics*, *Phys. Rev. Lett.* **48** (1982) 223.

[3] S. Borgani, A. Masiero, and M. Yamaguchi, *Light gravitinos as mixed dark matter*, *Phys. Lett.* **B386** (1996) 189–197, [hep-ph/9605222].

[4] S. A. Bonometto, F. Gabbiani, and A. Masiero, *A monochromatic axino dominated Universe*, *Phys. Lett.* **B222** (1989) 433–437.

[5] L. Covi, J. E. Kim, and L. Roszkowski, *Axinos as cold dark matter*, *Phys. Rev. Lett.* **82** (1999) 4180–4183, [hep-ph/9905212].

[6] F. D. Steffen, *Supersymmetric Dark Matter Candidates - The Lightest Neutralino, the Gravitino, and the Axino*, arXiv:0711.1240.

[7] B. C. Allanach, A. Dedes, and H. K. Dreiner, *The R parity violating minimal supergravity model*, *Phys. Rev.* **D69** (2004) 115002, [hep-ph/0309196].

[8] B. C. Allanach, M. A. Bernhardt, H. K. Dreiner, C. H. Kom, and P. Richardson, *Mass spectrum in R-parity violating mSUGRA and benchmark points*, *Phys. Rev.* **D75** (2007) 035002, [hep-ph/0609263].

[9] B. C. Allanach *et. al.*, *R-Parity violating minimal supergravity at the LHC*, arXiv:0710.2034.

[10] F. Takayama and M. Yamaguchi, *Gravitino dark matter without R-parity*, *Phys. Lett.* **B485** (2000) 388–392, [hep-ph/0005214].

[11] W. Buchmüller, L. Covi, K. Hamaguchi, A. Ibarra, and T. Yanagida, *Gravitino dark matter in R-parity breaking vacua*, *JHEP* **03** (2007) 037, [hep-ph/0702184].

[12] M. Drees and X. Tata, *Signals for heavy exotics at hadron colliders and supercolliders*, *Phys. Lett.* **B252** (1990) 695–702.

[13] A. Nisati, S. Petrarca, and G. Salvini, *On the possible detection of massive stable exotic particles at the LHC*, *Mod. Phys. Lett.* **A12** (1997) 2213–2222, [hep-ph/9707376].

[14] J. L. Feng and T. Moroi, *Tevatron signatures of long-lived charged sleptons in gauge-mediated supersymmetry breaking models*, *Phys. Rev.* **D58** (1998) 035001, [hep-ph/9712499].

[15] S. Ambrosanio, B. Mele, S. Petrarca, G. Polesello, and A. Rimoldi, *Measuring the SUSY breaking scale at the LHC in the slepton NLSP scenario of GMSB models*, *JHEP* **01** (2001) 014, [hep-ph/0010081].

[16] W. Buchmüller, K. Hamaguchi, M. Ratz, and T. Yanagida, *Supergravity at colliders*, *Phys. Lett.* **B588** (2004) 90–98, [hep-ph/0402179].

[17] K. Hamaguchi, Y. Kuno, T. Nakaya, and M. M. Nojiri, *A study of late decaying charged particles at future colliders*, *Phys. Rev.* **D70** (2004) 115007, [hep-ph/0409248].

[18] J. L. Feng and B. T. Smith, *Slepton trapping at the Large Hadron and International Linear Colliders*, *Phys. Rev.* **D71** (2005) 015004, [hep-ph/0409278].

[19] A. Brandenburg, L. Covi, K. Hamaguchi, L. Roszkowski, and F. D. Steffen, *Signatures of axinos and gravitinos at colliders*, *Phys. Lett.* **B617** (2005) 99–111, [hep-ph/0501287].

[20] A. De Roeck *et. al.*, *Supersymmetric benchmarks with non-universal scalar masses or gravitino dark matter*, *Eur. Phys. J.* **C49** (2007) 1041–1066, [hep-ph/0508198].

[21] H. U. Martyn, *Detecting metastable staus and gravitinos at the ILC*, *Eur. Phys. J.* **C48** (2006) 15–24, [hep-ph/0605257].

[22] F. D. Steffen, *Gravitino dark matter and cosmological constraints*, *JCAP* **0609** (2006) 001, [hep-ph/0605306].

[23] J. R. Ellis, A. R. Raklev, and O. K. Oye, *Gravitino dark matter scenarios with massive metastable charged sparticles at the LHC*, *JHEP* **10** (2006) 061, [hep-ph/0607261].

[24] K. Hamaguchi, M. M. Nojiri, and A. de Roeck, *Prospects to study a long-lived charged next lightest supersymmetric particle at the LHC*, *JHEP* **03** (2007) 046, [hep-ph/0612060].

[25] M. Bolz, A. Brandenburg, and W. Buchmüller, *Thermal production of gravitinos*, *Nucl. Phys.* **B606** (2001) 518–544, [hep-ph/0012052].

[26] A. Brandenburg and F. D. Steffen, *Axino dark matter from thermal production*, *JCAP* **0408** (2004) 008, [hep-ph/0405158].

[27] J. Pradler and F. D. Steffen, *Thermal gravitino production and collider tests of leptogenesis*, *Phys. Rev.* **D75** (2007) 023509, [hep-ph/0608344].

[28] V. S. Rychkov and A. Strumia, *Thermal production of gravitinos*, *Phys. Rev.* **D75** (2007) 075011, [hep-ph/0701104].

[29] R. H. Cyburt, J. R. Ellis, B. D. Fields, and K. A. Olive, *Updated nucleosynthesis constraints on unstable relic particles*, *Phys. Rev.* **D67** (2003) 103521, [astro-ph/0211258].

[30] M. Kawasaki, K. Kohri, and T. Moroi, *Big-bang nucleosynthesis and hadronic decay of long-lived massive particles*, *Phys. Rev.* **D71** (2005) 083502, [astro-ph/0408426].

[31] K. Jedamzik, *Big bang nucleosynthesis constraints on hadronically and electromagnetically decaying relic neutral particles*, *Phys. Rev.* **D74** (2006) 103509, [hep-ph/0604251].

[32] M. Kawasaki, K. Kohri, T. Moroi, and A. Yotsuyanagi, *Big-Bang Nucleosynthesis and Gravitino*, arXiv:0804.3745.

[33] M. Pospelov, *Particle physics catalysis of thermal big bang nucleosynthesis*, *Phys. Rev. Lett.* **98** (2007) 231301, [hep-ph/0605215].

[34] C. Bird, K. Koopmans, and M. Pospelov, *Primordial Lithium Abundance in Catalyzed Big Bang Nucleosynthesis*, hep-ph/0703096.

[35] M. Pospelov, *Bridging the primordial A=8 divide with Catalyzed Big Bang Nucleosynthesis*, arXiv:0712.0647.

[36] M. Pospelov, J. Pradler, and F. D. Steffen, *Constraints on Supersymmetric Models from Catalytic Primordial Nucleosynthesis of Beryllium*, arXiv:0807.4287.

[37] T. Asaka, K. Hamaguchi, and K. Suzuki, *Cosmological gravitino problem in gauge mediated supersymmetry breaking models*, *Phys. Lett.* **B490** (2000) 136–146, [hep-ph/0005136].

[38] M. Fujii, M. Ibe, and T. Yanagida, *Upper bound on gluino mass from thermal leptogenesis*, *Phys. Lett.* **B579** (2004) 6–12, [hep-ph/0310142].

[39] F. D. Steffen, *Constraints on gravitino dark matter scenarios with long- lived charged sleptons*, *AIP Conf. Proc.* **903** (2007) 595–598, [hep-ph/0611027].

[40] J. Pradler and F. D. Steffen, *Constraints on the reheating temperature in gravitino dark matter scenarios*, *Phys. Lett.* **B648** (2007) 224–235, [hep-ph/0612291].

[41] J. Pradler and F. D. Steffen, *Implications of Catalyzed BBN in the CMSSM with Gravitino Dark Matter*, *Phys. Lett.* **B666** (2008) 181–184, [arXiv:0710.2213].

[42] J. Pradler and F. D. Steffen, *CBBN in the CMSSM*, *Eur. Phys. J.* **C56** (2008) 287–291, [arXiv:0710.4548].

[43] M. Fukugita and T. Yanagida, *Baryogenesis without grand unification*, *Phys. Lett.* **B174** (1986) 45.

[44] S. Davidson and A. Ibarra, *A lower bound on the right-handed neutrino mass from leptogenesis*, *Phys. Lett.* **B535** (2002) 25–32, [hep-ph/0202239].

[45] W. Buchmüller, P. Di Bari, and M. Plümacher, *Leptogenesis for pedestrians*, *Ann. Phys.* **315** (2005) 305–351, [hep-ph/0401240].

[46] S. Blanchet and P. Di Bari, *Flavor effects on leptogenesis predictions*, *JCAP* **0703** (2007) 018, [hep-ph/0607330].

[47] S. Antusch and A. M. Teixeira, *Towards constraints on the susy seesaw from flavour-dependent leptogenesis*, *JCAP* **0702** (2007) 024, [hep-ph/0611232].

[48] R. H. Cyburt, J. R. Ellis, B. D. Fields, K. A. Olive, and V. C. Spanos, *Bound-state effects on light-element abundances in gravitino dark matter scenarios*, *JCAP* **0611** (2006) 014, [astro-ph/0608562].

[49] F. Takayama, *Extremely Long-Lived Charged Massive Particles as a Probe for Reheating of the Universe*, *Phys. Rev.* **D77** (2008) 116003, [arXiv:0704.2785].

[50] K. Hamaguchi, T. Hatsuda, M. Kamimura, Y. Kino, and T. T. Yanagida, *Stau-catalyzed Li-6 production in big-bang nucleosynthesis*, *Phys. Lett.* **B650** (2007) 268–274, [hep-ph/0702274].

[51] A. Djouadi, J.-L. Kneur, and G. Moultaka, *Suspect: A fortran code for the supersymmetric and higgs particle spectrum in the mssm*, *Comput. Phys. Commun.* **176** (2007) 426–455, [hep-ph/0211331].

[52] C. F. Berger, L. Covi, S. Kraml, and F. Palorini, *The number density of a charged relic*, *JCAP* **0810** (2008) 005, [arXiv:0807.0211].

[53] G. Belanger, F. Boudjema, A. Pukhov, and A. Semenov, *micrOMEGAs: A program for calculating the relic density in the MSSM*, *Comput. Phys. Commun.* **149** (2002) 103–120, [hep-ph/0112278].

[54] G. Belanger, F. Boudjema, A. Pukhov, and A. Semenov, *MicrOMEGAs: Version 1.3*, *Comput. Phys. Commun.* **174** (2006) 577–604, [hep-ph/0405253].

[55] G. Belanger, F. Boudjema, A. Pukhov, and A. Semenov, *micrOMEGAs 2.0.7: A program to calculate the relic density of dark matter in a generic model*, *Comput. Phys. Commun.* **177** (2007) 894–895.

[56] G. Belanger, F. Boudjema, A. Pukhov, and A. Semenov, *Dark matter direct detection rate in a generic model with micrOMEGAs2.1*, arXiv:0803.2360.

[57] J. Kersten and K. Schmidt-Hoberg, *The Gravitino-Stau Scenario after Catalyzed BBN*, *JCAP* **0801** (2008) 011, [arXiv:0710.4528].

[58] P. Gondolo and G. Gelmini, *Cosmic abundances of stable particles: Improved analysis*, *Nucl. Phys.* **B360** (1991) 145–179.

[59] J. R. Ellis, T. Falk, K. A. Olive, and M. Srednicki, *Calculations of neutralino stau coannihilation channels and the cosmologically relevant region of MSSM parameter space*, *Astropart. Phys.* **13** (2000) 181–213, [hep-ph/9905481].

[60] T. Hahn, *Generating Feynman diagrams and amplitudes with FeynArts 3*, *Comput. Phys. Commun.* **140** (2001) 418–431, [hep-ph/0012260].

[61] T. Hahn and C. Schappacher, *The implementation of the minimal supersymmetric standard model in FeynArts and FormCalc*, *Comput. Phys. Commun.* **143** (2002) 54–68, [hep-ph/0105349].

[62] T. Hahn and M. Perez-Victoria, *Automatized one-loop calculations in four and D dimensions*, *Comput. Phys. Commun.* **118** (1999) 153–165, [hep-ph/9807565].

[63] T. Hahn and M. Rauch, *News from FormCalc and LoopTools*, *Nucl. Phys. Proc. Suppl.* **157** (2006) 236–240, [hep-ph/0601248].

[64] M. Abramowitz and I. A. Stegun, *Handbook of Mathematical Functions with Formulas, Graphs, and Mathematical Tables*. Dover, New York, tenth ed., 1964.

[65] P. Gondolo *et. al.*, *DarkSUSY: Computing supersymmetric dark matter properties numerically*, *JCAP* **0407** (2004) 008, [astro-ph/0406204].

[66] S. Heinemeyer, W. Hollik, and G. Weiglein, *FeynHiggs: A program for the calculation of the masses of the neutral CP-even Higgs bosons in the MSSM*, *Comput. Phys. Commun.* **124** (2000) 76–89, [hep-ph/9812320].

[67] G. Belanger, F. Boudjema, A. Pukhov, and A. Semenov, *micrOMEGAs2.0: A program to calculate the relic density of dark matter in a generic model*, *Comput. Phys. Commun.* **176** (2007) 367–382, [hep-ph/0607059].

[68] A. Pukhov, *CalcHEP 3.2: MSSM, structure functions, event generation, batchs, and generation of matrix elements for other packages*, hep-ph/0412191.

[69] M. N. Dubinin and A. V. Semenov, *Triple and quartic interactions of Higgs bosons in the general two-Higgs-doublet model*, hep-ph/9812246.

[70] J. F. Gunion and H. E. Haber, *The CP-conserving two-Higgs-doublet model: The approach to the decoupling limit*, *Phys. Rev.* **D67** (2003) 075019, [hep-ph/0207010].

[71] H. E. Haber, *Higgs boson masses and couplings in the minimal supersymmetric model*, hep-ph/9707213.

[72] M. S. Carena, J. R. Espinosa, M. Quiros, and C. E. M. Wagner, *Analytical expressions for radiatively corrected Higgs masses and couplings in the MSSM*, *Phys. Lett.* **B355** (1995) 209–221, [hep-ph/9504316].

[73] J. A. Casas, A. Lleyda, and C. Munoz, *Strong constraints on the parameter space of the MSSM from charge and color breaking minima*, *Nucl. Phys.* **B471** (1996) 3–58, [hep-ph/9507294].

[74] K. Griest and M. Kamionkowski, *Unitarity Limits on the Mass and Radius of Dark Matter Particles*, *Phys. Rev. Lett.* **64** (1990) 615.

[75] E. Boos, A. Djouadi, M. Mühlleitner, and A. Vologdin, *The MSSM Higgs bosons in the intense-coupling regime*, *Phys. Rev.* **D66** (2002) 055004, [hep-ph/0205160].

[76] E. Boos, A. Djouadi, and A. Nikitenko, *Detection of the neutral MSSM Higgs bosons in the intense- coupling regime at the LHC*, *Phys. Lett.* **B578** (2004) 384–393, [hep-ph/0307079].

[77] A. Djouadi, *The anatomy of electro-weak symmetry breaking. II: The Higgs bosons in the minimal supersymmetric model*, *Phys. Rept.* **459** (2008) 1–241, [hep-ph/0503173].

[78] M. S. Carena, S. Heinemeyer, C. E. M. Wagner, and G. Weiglein, *Suggestions for improved benchmark scenarios for Higgs- boson searches at LEP2*, hep-ph/9912223.

[79] K. Griest and D. Seckel, *Three exceptions in the calculation of relic abundances*, *Phys. Rev.* **D43** (1991) 3191–3203.

[80] W. Porod, *SPheno, a program for calculating supersymmetric spectra, SUSY particle decays and SUSY particle production at e^+e^- colliders*, *Comput. Phys. Commun.* **153** (2003) 275–315, [hep-ph/0301101].

[81] F. Mahmoudi, *New constraints on supersymmetric models from $b \to s$ gamma*, *JHEP* **12** (2007) 026, [arXiv:0710.3791].

[82] G. Degrassi, S. Heinemeyer, W. Hollik, P. Slavich, and G. Weiglein, *Towards high-precision predictions for the MSSM Higgs sector*, *Eur. Phys. J.* **C28** (2003) 133–143, [hep-ph/0212020].

[83] M. Drees and M. M. Nojiri, *One loop corrections to the Higgs sector in minimal supergravity models*, *Phys. Rev.* **D45** (1992) 2482–2492.

[84] M. Drees and S. P. Martin, *Implications of SUSY model building*, hep-ph/9504324.

[85] M. S. Carena, M. Olechowski, S. Pokorski, and C. E. M. Wagner, *Electroweak symmetry breaking and bottom - top Yukawa unification*, *Nucl. Phys.* **B426** (1994) 269–300, [hep-ph/9402253].

[86] J. L. Feng, S. Su, and F. Takayama, *Supergravity with a gravitino LSP*, *Phys. Rev.* **D70** (2004) 075019, [hep-ph/0404231].

[87] A. Datta, A. Djouadi, and J.-L. Kneur, *Probing the SUSY Higgs boson couplings to scalar leptons at high-energy e^+e^- colliders*, *Phys. Lett.* **B509** (2001) 299–306, [hep-ph/0101353].

[88] S. Dittmaier, M. Kramer, and M. Spira, *Higgs radiation off bottom quarks at the Tevatron and the LHC*, *Phys. Rev.* **D70** (2004) 074010, [hep-ph/0309204].

[89] S. Dawson, C. B. Jackson, L. Reina, and D. Wackeroth, *Exclusive Higgs boson production with bottom quarks at hadron colliders*, *Phys. Rev.* **D69** (2004) 074027, [hep-ph/0311067].

[90] R. V. Harlander and W. B. Kilgore, *Higgs boson production in bottom quark fusion at next-to- next-to-leading order*, *Phys. Rev.* **D68** (2003) 013001, [hep-ph/0304035].

[91] S. Dittmaier, M. Kramer, A. Muck, and T. Schlüter, *MSSM Higgs-boson production in bottom-quark fusion: Electroweak radiative corrections*, *JHEP* **03** (2007) 114, [hep-ph/0611353].

[92] **CMS** Collaboration, G. L. Bayatian *et. al.*, *CMS technical design report, volume II: Physics performance*, *J. Phys.* **G34** (2007) 995–1579.

[93] F. D. Steffen, *Probing the Reheating Temperature at Colliders and with Primordial Nucleosynthesis*, *Phys. Lett.* **B669** (2008) 74–80, [arXiv:0806.3266].

[94] T. Asaka, S. Nakamura, and M. Yamaguchi, *Gravitinos from heavy scalar decay*, *Phys. Rev.* **D74** (2006) 023520, [hep-ph/0604132].

[95] M. Endo, F. Takahashi, and T. T. Yanagida, *Inflaton Decay in Supergravity*, *Phys. Rev.* **D76** (2007) 083509, [arXiv:0706.0986].

[96] M. Ratz, K. Schmidt-Hoberg, and M. W. Winkler, *A note on the primordial abundance of stau NLSPs*, arXiv:0808.0829.

Table 2: Exemplary CMSSM points A, B, and C shown in Figs. 6 and 7. In addition to the quantities explained in the main text, values of the gluino mass $m_{\widetilde{g}}$ and of the mass of the lighter stop $m_{\widetilde{t}_1}$ are given together with the relative importance of the dominant stau annihilation channels, $x_{\rm f} = m_{\widetilde{\tau}_1}/T_{\rm f}$, and the decoupling yield $Y_{\widetilde{\tau}}$. For each point, we list gravitino dark matter scenarios with $m_{\widetilde{G}} = 100$ (50) GeV and associated values of the stau lifetime $\tau_{\widetilde{\tau}_1}$, the non-thermally produced gravitino density $\Omega_{\widetilde{G}}^{\rm NTP}h^2$, and the maximum reheating temperature $T_{\rm R}^{\rm max}$.

Point		A	B	C
$m_{1/2}$	[GeV]	456	600	1138
m_0	[GeV]	124	748	30
$\tan\beta$		43	55	55
$m_{\widetilde{\tau}_1}$	[GeV]	130	197	127
$m_{\widetilde{\tau}_2}$	[GeV]	352	673	739
$\theta_{\widetilde{\tau}}$		114	80	75
m_{h^0}	[GeV]	114.6	115	117.9
m_{H^0,A^0}	[GeV]	265	390	799
Γ_{H^0}	[GeV]	9.6	22	41
μ	[GeV]	-565	666	1262
A_τ	[GeV]	-63	473	-164
$m_{\widetilde{g}}$	[GeV]	1052	1375	2446
$m_{\widetilde{t}_1}$	[GeV]	740	1091	1757
$b\overline{b}$	[%]	76	87	< 1
h^0h^0	[%]	10	< 1	90
$\tau\overline{\tau}$	[%]	9	11	< 1
WW	[%]	2	< 1	6
$x_{\rm f}$		30	30	32
$Y_{\widetilde{\tau}}$	$[10^{-15}]$	4.2	2.5	2.2
$m_{\widetilde{G}}$	[GeV]	100 (50)	100 (50)	100 (50)
$\tau_{\widetilde{\tau}_1}$	[s]	5.7×10^9 (7.5×10^7)	6.5×10^7 (6.4×10^6)	8.5×10^9 (8.7×10^7)
$\Omega_{\widetilde{G}}^{\rm NTP}h^2$	$[10^{-4}]$	1.2 (0.58)	0.7 (0.35)	0.64 (0.32)
$T_{\rm R}^{\rm max}$	[GeV]	1.9×10^9 (9.5×10^8)	1.1×10^9 (5.5×10^8)	3.1×10^8 (1.5×10^8)